nature neuroscience

ARTICLES

https://doi.org/10.1038/s41593-020-0637-3

Motor learning promotes remyelination via new and surviving oligodendrocytes

Clara M. Bacmeister[1,4], Helena J. Barr[1,4], Crystal R. McClain[1,4], Michael A. Thornton[1], Dailey Nettles[1,2,3], Cristin G. Welle[2,3] and Ethan G. Hughes[1]✉

Oligodendrocyte loss in neurological disease leaves axons vulnerable to damage and degeneration, and activity-dependent myelination may represent an endogenous mechanism to improve remyelination following injury. Here we report that, while learning a forelimb reach task transiently suppresses oligodendrogenesis, it subsequently increases oligodendrocyte precursor cell differentiation, oligodendrocyte generation and myelin sheath remodeling in the forelimb motor cortex. Immediately following demyelination, neurons exhibit hyperexcitability, learning is impaired and behavioral intervention provides no benefit to remyelination. However, partial remyelination restores neuronal and behavioral function, allowing learning to enhance oligodendrogenesis, remyelination of denuded axons and the ability of surviving oligodendrocytes to generate new myelin sheaths. Previously considered controversial, we show that sheath generation by mature oligodendrocytes is not only possible but also increases myelin pattern preservation following demyelination, thus presenting a new target for therapeutic interventions. Together, our findings demonstrate that precisely timed motor learning improves recovery from demyelinating injury via enhanced remyelination from new and surviving oligodendrocytes.

Oligodendrocytes, the myelin-forming cells of the CNS, enhance the propagation of action potentials and support neuronal and axonal integrity through metabolic coupling. Injury to oligodendrocytes critically affects axonal health and is associated with significant neurological disability in patients with multiple sclerosis (MS)[1]. While a growing number of immunotherapies decrease the frequency of MS attacks, they do not fully prevent axonal degeneration or the accumulation of disability[2]. Oligodendrocyte precursor cells (OPCs) can generate new oligodendrocytes with the capacity to remyelinate denuded axons, which can restore neuronal function[3,4]. However, remyelination is typically incomplete in patients with MS[5], and approaches to increase myelin repair remain limited[6]. Interestingly, recent studies have shown that oligodendrocyte turnover varies considerably among patients with MS and posit a controversial role for preexisting oligodendrocytes in remyelination[7,8]. While current dogma maintains that mature oligodendrocytes do not participate in remyelination[9], recent evidence from large animal models of demyelinating injury suggests that myelinating oligodendrocytes may make new myelin sheaths[10]. Furthermore, neuronal activity can modify myelin sheaths via adjustments to internode length and thickness, which raises the possibility that mature oligodendrocytes can alter their myelination in an activity-dependent manner[11]. Together, these findings suggest the existence of endogenous mechanisms that may modulate myelin repair by new and surviving oligodendrocytes following demyelinating injury.

Motor learning drives white matter changes in humans and rodents in part by eliciting the proliferation and differentiation of OPCs in the adult CNS[12,13], similar to OPC responses to demyelinating injuries[4]; however, it remains unclear whether learning during demyelination has synergistic or antagonistic effects. Personalized behavioral interventions are increasingly being used in clinical settings to ameliorate motor function in patients with myelin disease[14]. Optimizing the modality and timing of behavioral interventions may allow endogenous mechanisms of myelin plasticity to act in synchrony and drive more robust remyelination following injury.

Through longitudinal in vivo two-photon imaging of oligodendrocyte lineage cells and individual myelin sheaths, we defined the complex dynamics between motor skill acquisition and oligodendroglia in the motor cortex. We studied this in both developmental and remyelinating contexts using the cuprizone-mediated demyelination model, which results in ongoing oligodendrocyte death and regeneration similar to cortical lesions in patients with MS[15], but without the confound of autoimmunity. We found that motor learning, when properly timed, enhances oligodendrogenesis after injury and recruits mature oligodendrocytes to participate in remyelination through the generation of new myelin sheaths.

Results

Forelimb reach training dynamically modulates oligodendrocyte lineage cells and myelination. Previous assessments using cell lineage tracing and stage-specific markers[16,17] indicated that motor learning rapidly increases adult oligodendrogenesis; however, the dynamics of activity-dependent myelination remain unclear due to incomplete labeling of differentiating OPC populations and interindividual variability in cross-sectional approaches. To determine the dynamics of oligodendrocytes, myelin and OPCs during learning, we used longitudinal two-photon in vivo imaging in the forelimb region of the motor cortex throughout the learning and rehearsal of a skilled, single-pellet contralateral forelimb reach task[18] (Fig. 1a,b; Extended Data Fig. 1; Supplementary Video 1). We used transgenic mice that express enhanced green fluorescent protein (EGFP) in all cortical myelinating oligodendrocytes and myelin sheaths[19] (*MOBP–EGFP* mice; Fig. 1c; Supplementary Video 2) to examine the effects of learning on oligodendrogenesis and

[1]Department of Cell and Developmental Biology, University of Colorado School of Medicine, Aurora, CO, USA. [2]Department of Neurosurgery, University of Colorado School of Medicine, Aurora, CO, USA. [3]Department of Physiology and Biophysics, University of Colorado School of Medicine, Aurora, CO, USA. [4]These authors contributed equally: Clara M. Bacmeister, Helena J. Barr, Crystal R. McClain. ✉e-mail: ethan.hughes@cuanschutz.edu

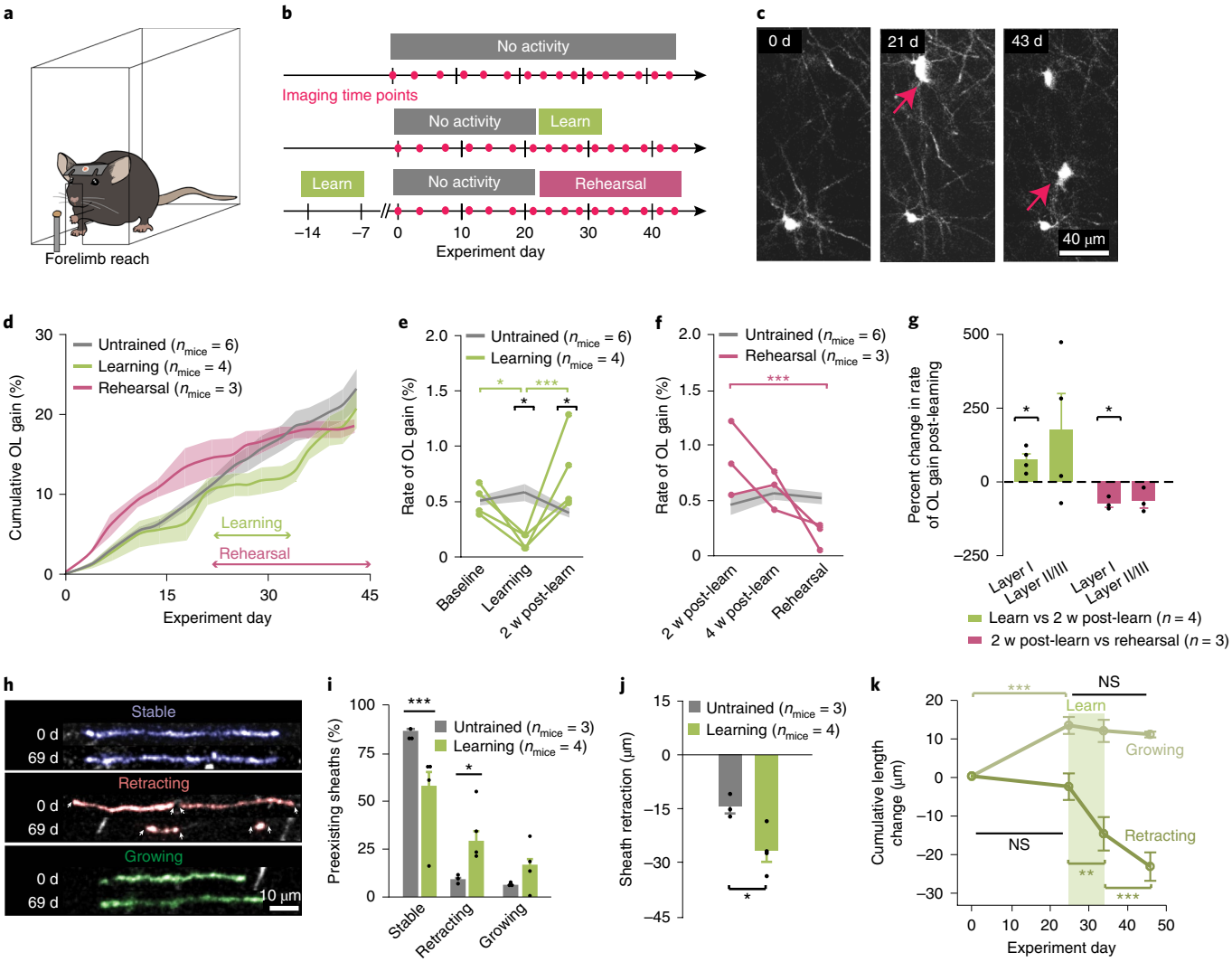

Fig. 1 | Forelimb reach training modulates oligodendrogenesis and remodeling of preexisting myelin sheaths. a,**b**, Illustration (**a**) and imaging timeline (**b**) of behavioral interventions. **c**, Example of motor cortex oligodendrogenesis, whereby the red arrows indicate new cells. d, day. **d**, Cumulative gain in oligodendrocytes (OLs) by group, as assessed as percentage increase from baseline (mean ± s.e.m.). **e**, Learning modulates oligodendrogenesis rate ($F_{2,16}$ = 15.61, P = 0.0002; the gray line and shaded area represent the mean ± s.e.m., respectively, of controls; green traces represent individual learning mice). The rate is suppressed during learning relative to baseline (P = 0.046; Tukey's HSD), resulting in a decreased rate relative to controls (P = 0.016). The rate increases in the 2 weeks post-learning (2 w post-learn; P = 0.0005; Tukey's HSD), resulting in a higher rate than controls (P = 0.05). **f**, Rehearsal modulates oligodendrogenesis rate ($F_{2,14}$ = 10.33, P = 0.002; the gray line and shaded area represents the mean ± s.e.m., respectively, of controls; pink traces represent individual rehearsal mice). The rate decreases between 2 weeks post-learning and rehearsal (P = 0.0009; Tukey's HSD), but does not differ between untrained and rehearsal mice. **g**, Non-zero changes in oligodendrogenesis rate (both the increase 2 weeks post-learning and decrease during rehearsal) are restricted to layer I of the cortex (one sample t-test; P = 0.037 and P = 0.027, respectively; points represent individual mice). **h**,**i**, Learning modulates preexisting sheath stability (percentage; $F_{5,42}$ = 69.72, P < 0.0001; points represent means per mouse). Learning mice have fewer stable sheaths (P < 0.0001; Tukey's HSD) and more retracting sheaths (P = 0.014; white arrows indicate paranodes of individual sheaths, and sheaths are pseudocolored in **h**). **j**, Sheaths retract further in learning versus untrained mice (n_{mice} = 4, $n_{sheaths}$ = 59 and n_{mice} = 3, $n_{sheaths}$ = 22, respectively; Student's t-test, t(4.62) = 3.32, P = 0.02). **k**, Growing sheaths lengthen before learning (Wilcoxon signed-rank; P = 0.00006), but cease growth after the onset of learning. Retracting sheaths are initially stable, but retract during (P = 0.0047) and after learning (P = 0.019). *P < 0.05, **P < 0.01, ***P < 0.001, NS, not significant; bars and error bars represent the mean ± s.e.m. For detailed statistics, see Supplementary Table 2, tab 1.

preexisting myelin sheath remodeling in healthy mice. Long-term in vivo imaging of layers I–III allowed us to track ~100 oligodendrocytes and their myelin sheaths over the course of 2–3 months per mouse. Immunohistochemistry, in vivo spectral confocal reflectance (SCoRe) microscopy imaging and semiautomated tracing confirmed that EGFP in *MOBP–EGFP* transgenic mice faithfully reflects the presence and length of myelin sheaths and allows morphological reconstruction of individual oligodendrocytes (using Simple Neurite Tracer[20]; Extended Data Fig. 2; Supplementary Video 3). Assuming a range of 45 ± 4 sheaths per cortical oligodendrocyte[19], our average sampling was 67–74% of an individual oligodendrocyte arbor.

To separate the effects of motor learning from performance, we performed in vivo imaging during initial training ('learning'; 7 days of 20-min sessions) and during performance of the task 1 month post-training ('rehearsal'; 5 days of 20-min sessions for 3 weeks; Fig. 1b). Of all the trained mice, 93% were able to learn the task, and both learning and rehearsal of the task resulted in skill refinement

(Extended Data Fig. 1). We trained mice between 2 and 3 months old, when oligodendrogenesis is ongoing (Extended Data Fig. 3).

We found that learning the reach task transiently decreased and subsequently increased the rate of oligodendrogenesis in the forelimb motor cortex (Fig. 1d,e). During learning, oligodendrogenesis rate decreased by ~75% relative to age-matched controls (0.14 ± 0.03% versus 0.58 ± 0.08%, respectively; rate refers to the percentage increase in oligodendrocytes over the number of days elapsed). Suppression of oligodendrogenesis was restricted to the training period and was not mediated by the effects of handling (all mice were handled equally) or training-related diet restriction (Extended Data Fig. 3). Immediately following learning, oligodendrogenesis rate increased, resulting in an almost twofold greater rate of oligodendrogenesis relative to untrained controls (0.77 ± 0.19% versus 0.40 ± 0.04, respectively; Fig. 1e), and remained elevated for 3 weeks (Extended Data Fig. 3). Proficiency in the reach task predicted the magnitude of oligodendrogenesis rate increase following learning (Extended Data Fig. 3). In contrast, rehearsal of the task did not alter oligodendrogenesis rates relative to controls, and the post-learning burst in oligodendrogenesis eventually tapered off (Fig. 1f; Extended Data Fig. 3). Overall, mice that had been trained (both learning and rehearsal) had higher maximum rates of oligodendrogenesis than untrained mice (Extended Data Fig. 3). Only layer I of the forelimb motor cortex demonstrated consistent changes in the post-learning oligodendrogenesis rate (Fig. 1g); this brain region is where motor learning strengthens horizontal connections between neurons[21]. Oligodendrogenesis rate in layer II/III was variable among mice.

Next, we examined remodeling of preexisting myelin sheaths throughout learning. Under normal physiological conditions, a small number of myelin sheaths exhibited dynamic length changes, similar to previous descriptions in young adult mice[22] (14.7 ± 1.71%; Fig. 1h,i; Supplementary Videos 4 and 5). One week post-learning, the proportion of dynamic preexisting myelin sheaths increased in learning mice relative to controls (43.46 ± 7.82% versus 14.74 ± 1.71%). Learning increased both the proportion of sheaths that underwent retraction and the distance that these sheaths retracted compared with untrained mice (Fig. 1i,j). Learning also modulated the timing of sheath remodeling, whereby growing sheaths ceased to lengthen at the onset of learning, while learning induced the retraction of previously stable sheaths (Fig. 1k). We found no evidence to indicate that new myelin sheaths were generated by preexisting oligodendrocytes in untrained or learning mice.

To further characterize how motor skill learning modulates the generation of new mature oligodendrocytes, we used longitudinal in vivo two-photon imaging of transgenic mice that express membrane-anchored EGFP in OPCs (*NG2–mEGFP* mice[23]) to track OPC migration, proliferation, differentiation and death in the forelimb motor cortex over 5 weeks, beginning 1 week before forelimb reach training (Fig. 2a,b). Similar to oligodendrogenesis, learning induced a twofold increase in the rate of OPC differentiation in the week following learning (0.59 ± 0.10% during learning versus 1.23 ± 0.19% post-learning; Fig. 2c); however, the OPC differentiation rate was unaffected during reach training. Neither the rates of proliferation nor death differed significantly across the 5 weeks (Fig. 2d,e). However, five out of five mice displayed a reduction in proliferation rate (~50%) during learning relative to baseline (Extended Data Fig. 3). Our previous work indicated that the majority of adult OPC differentiation events occur via direct differentiation rather than asymmetric cell division[23]. In line with these findings, only 10.91 ± 3.77% of differentiating OPCs had previously proliferated during the 5 weeks of observation. The proportion of asymmetric differentiation events was unaffected by motor learning (Fig. 2a,f,g). To assess whether the increase in OPC differentiation following motor learning was due to parenchymal OPCs or precursors recruited from nearby brain regions or germinal zones, we tracked OPCs that migrated into the imaging volume (Extended Data Fig. 3). Migration into the field was rare, with 4.68 ± 0.96% of the baseline number of OPCs migrating in and 2.73 ± 0.36% migrating out, and this was not altered by learning. Only 3.57 ± 1.49% of the total proliferation events and 0.70 ± 0.30% of the total differentiation events occurred in cells that migrated into the imaging volume. These data indicate that parenchymal OPCs residing in the motor cortex directly differentiated following acquisition of the reach task.

Demyelination results in incomplete oligodendrocyte replacement, changes to the pattern of myelination and functional deficits in the motor cortex. Gray matter lesions in patients with MS contain both dying and newly forming oligodendrocytes[15], a feature that has complicated the interpretation of remyelination in humans and in animal models of MS[24]. To visualize the dynamics of myelin loss and repair, we used longitudinal two-photon in vivo imaging during cuprizone-mediated demyelination (Fig. 3a; Supplementary Video 6). We fed 10-week-old congenic *MOBP–EGFP* mice a 0.2% cuprizone diet for 3 weeks to induce oligodendrocyte death (~90% in the forelimb motor cortex; Fig. 3a–h), and confirmed that in vivo two-photon analysis of *MOBP–EGFP* mice is a reliable measure of oligodendrocyte and myelin sheath loss with SCoRe microscopy and immunohistochemistry (Extended Data Fig. 4). In contrast to the loss of myelin and mature oligodendrocytes, the number of cortical OPCs was unchanged following cuprizone administration relative to age-matched controls (138.63 ± 19.75 cells mm^{-2} versus 179.11 ± 14.99 cells mm^{-2}, respectively; Extended Data Fig. 4), which is similar to a recently published study[25].

Oligodendrocyte loss occurred evenly across cortical depths (Extended Data Fig. 5), leaving a small number of oligodendrocytes and myelin intact (12.94 ± 3.10%, 'surviving' oligodendrocytes; Fig. 3b,c). Cuprizone treatment suppressed oligodendrogenesis, and 85% of the few cells generated during cuprizone administration died within 3 weeks (Extended Data Fig. 5). Oligodendrocyte death followed a biphasic model of myelin loss (1.53 ± 1.27 days before cuprizone cessation) followed by cell body loss (7.26 ± 1.22 days post-cuprizone; Fig. 3d,e; Supplementary Video 7), which is similar to previous descriptions of demyelination occurring via a 'dying-back' process[26]. Oligodendrocyte loss plateaued approximately 15 days following the cessation of cuprizone administration (Fig. 3f). Removal of cuprizone from the diet induced a robust oligodendrogenesis response that was proportional to the extent of oligodendrocyte loss, and this response plateaued at approximately 3 weeks (Fig. 3f,g; Extended Data Fig. 5). The cortical distribution of newly generated oligodendrocytes was comparable between remyelinating and healthy conditions. Maximum oligodendrogenesis rates during remyelination were six times greater than in healthy untrained mice (5.95 ± 0.38% versus 0.99 ± 0.69%) and almost four times greater than in healthy trained mice (5.95 ± 0.38% versus 1.60 ± 0.64%; Extended Data Fig. 5).

To further characterize the oligodendrogenesis response, we tracked mice for up to 60 days after cuprizone cessation. Due to the oral uptake of cuprizone, there were inter-mouse variations in the extent of demyelination and, consequently, remyelination (Extended Data Fig. 5). We therefore quantified the number of oligodendrocytes generated during remyelination as a proportion of total oligodendrocyte loss ('oligodendrocyte replacement,' percentage; see Methods). Oligodendrocyte replacement after cuprizone cessation followed a sigmoidal pattern, and we quantified it using three-parameter (3P) logistic equations. We were specifically interested in the inflection point (when oligodendrogenesis switches from accelerating to decelerating) and the asymptote of the curve (the plateau of oligodendrocyte replacement; Supplementary Table 2). Oligodendrocyte replacement was delayed relative to loss by approximately 4 days and plateaued significantly

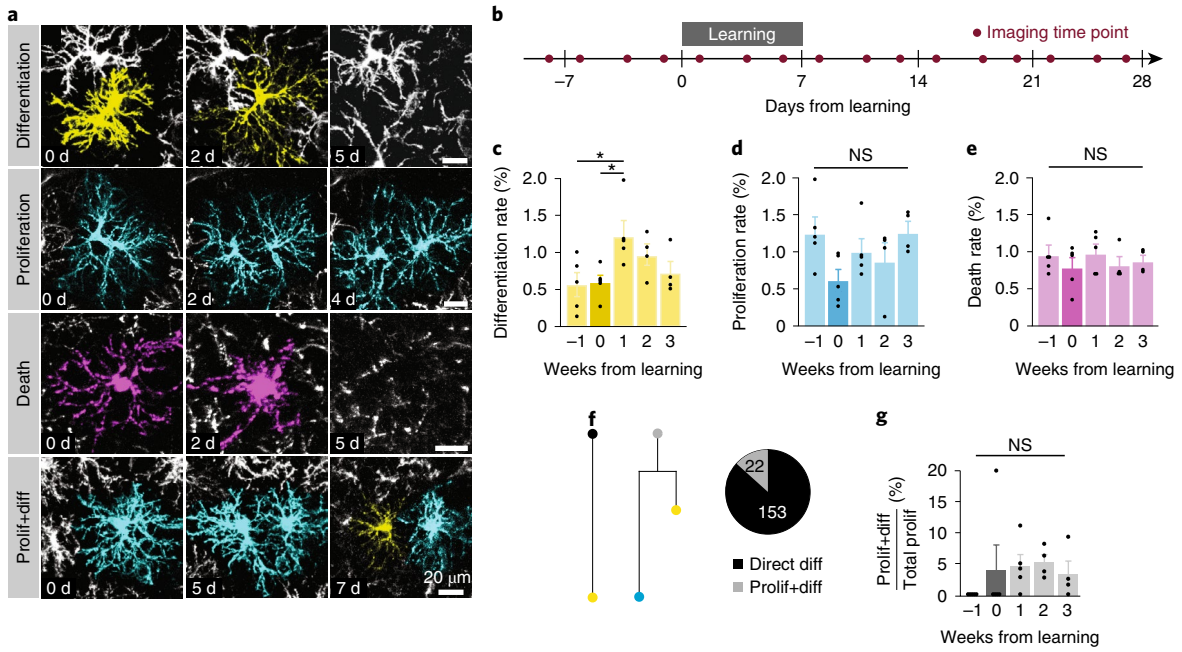

Fig. 2 | Forelimb reach learning increases OPC differentiation. a, In vivo imaging of EGFP$^+$ OPCs in 10-week-old *NG2-mEGFP* mice. OPCs that undergo differentiation (yellow; top row) retract their filopodia, increase branching and lose mEGFP fluorescence intensity while surrounding OPC processes infiltrate their domain. Proliferating OPCs (cyan; second row) undergo cytokinesis and migrate to form independent domains. Dying OPCs (magenta; third row) retract fragmented processes, and their cell bodies become enlarged before disappearance. A small percentage of OPCs undergo proliferation followed by differentiation (Prolif+diff; bottom row). **b**, Experimental timeline with imaging time points. **c**, The OPC differentiation rate varies by learning week (mean ± s.e.m.; $F_{4,14} = 4.85$, $P = 0.011$). The rate increases during the first week following forelimb reach training compared with both baseline and learning week ($P = 0.015$ and $P = 0.021$, respectively; Tukey's HSD). **d**, There is no effect of learning on the proliferation rate. **e**, There is no effect of learning on the death rate. **f**, Differentiating OPCs can either directly differentiate (direct diff, left cell-fate diagram) or undergo proliferation followed by differentiation of a daughter cell (prolif+diff, right cell-fate diagram). Cell-fate diagram colors (yellow, differentiation; blue, proliferation) correspond to cellular behaviors, as in **a**; 87.4% (153/175) of differentiating OPCs proceeded through direct differentiation. Pie chart colors (black and grey) correspond with the starting cells in fate diagrams at left. **g**, The proportion of differentiation events that occurred following cell division (prolif+diff) did not differ between baseline and learning or post-learning time points. $^*P < 0.05$, $^{**}P < 0.01$, $^{***}P < 0.001$; bars and error bars represent the mean ± s.e.m.; points represent individual mice. For detailed statistics, see Supplementary Table 2, tab 2.

lower than oligodendrocyte loss (Fig. 3h). Mice only replaced on average 60.52 ± 3.03% of lost oligodendrocytes in the 7 weeks post-cuprizone, and the remyelination response failed to restore baseline oligodendrocyte numbers.

To determine the effects of oligodendrocyte loss and incomplete replacement on neuronal function in the forelimb motor cortex, we performed chronic weekly in vivo extracellular recordings in both cuprizone-demyelinated and age-matched control mice. In vivo multisite electrodes record extracellular potentials from neurons within approximately a 150-μm radius of the recording electrode[27]. We confirmed via histology that the proportion of proximally myelinated neurons in this sampling radius was decreased by over 50% at the cessation of cuprizone administration relative to controls (Extended Data Fig. 5). Neuronal firing rates did not differ between groups before or during cuprizone administration, which is consistent with work in ex vivo cortical slices[28]. However, median neuronal firing rates were increased in demyelinated mice versus controls by ~70% in the first week and 40% in the second week post-cuprizone treatment (11.90 versus 6.92 Hz and 10.68 versus 7.69 Hz, respectively; Fig. 3i,j), which indicates that they were hyperexcitable in a manner that temporally correlates with maximum oligodendrocyte loss. By 3 and 4 weeks post-cuprizone treatment—when remyelination plateaued—neuronal firing rates in cuprizone-demyelinated mice were indistinguishable from age-matched controls. Taken together, these results demonstrate that cuprizone-mediated demyelination induces aberrant neuronal function in the forelimb region of the motor cortex that recovers synchronously with remyelination.

Given that remyelination failed to completely restore baseline oligodendrocyte numbers but seemed to restore neuronal function, we sought to examine the number, the length and the location of sheaths generated by new oligodendrocytes during remyelination. In the first week of remyelination, new oligodendrocytes formed more myelin sheaths than oligodendrocytes generated in the second week of remyelination or in control mice (54.4 ± 3.25 versus 39.4 ± 1.72 and 42.28 ± 1.30 total sheaths, respectively; Fig. 4a–c; Supplementary Videos 8 and 9). In healthy mice and during remyelination, sheaths from new oligodendrocytes stabilized to similar lengths within 3 days after generation (Fig. 4d–f). Therefore, the increased sheath number on new oligodendrocytes in the week following demyelination resulted in a larger total amount of myelin per oligodendrocyte (Fig. 4g). In addition, myelin sheaths of newly generated oligodendrocytes were more often placed in previously unmyelinated areas ('remodeling'; 67.7 ± 3.56% of sheaths) rather than in denuded areas ('remyelinating'; 32.0 ± 3.47% of sheaths), thus generating a novel pattern of myelination following demyelinating injury (Fig. 4h,i; Supplementary Videos 10 and 11). These findings indicate that the myelinating capacity of individual oligodendrocytes is increased during early remyelination, and that remyelination by new oligodendrocytes alters the pattern of cortical myelin.

Motor learning modulates oligodendrogenesis after demyelination in a timing-dependent manner. Since we found that motor learning increased both OPC differentiation and oligodendrogenesis

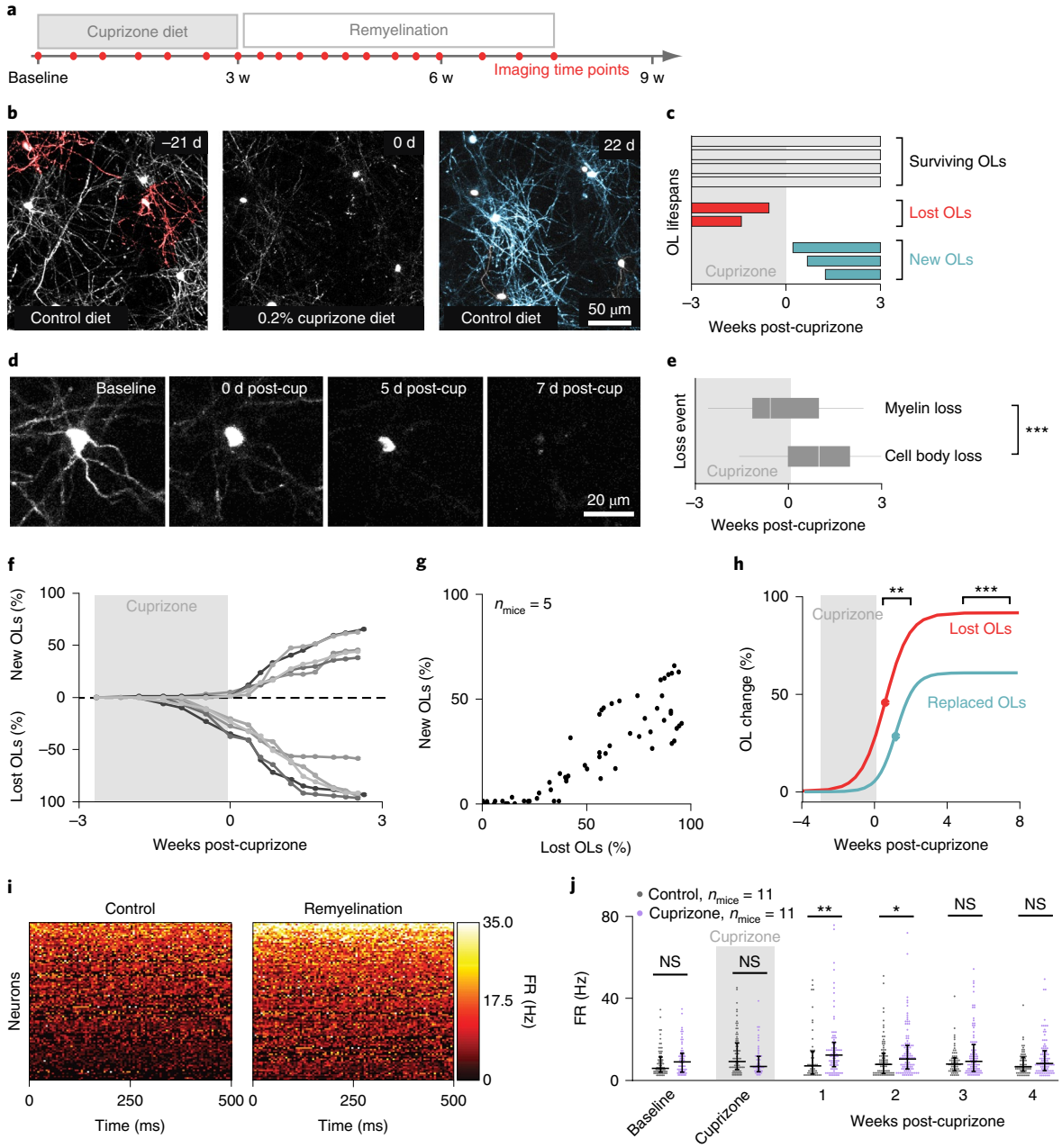

Fig. 3 | Demyelination results in incomplete oligodendrocyte replacement and functional deficits in motor cortex. a, Timeline of cuprizone administration and in vivo two-photon imaging. **b**,**c**, Representative images (**b**) and categorization (**c**) of OL fates following cuprizone administration as 'surviving' (gray), 'lost' (red) and 'new' (blue). Shaded area in **c** represents cuprizone administration. **d**,**e**, Representative images (**d**) and categorization (**e**) of biphasic OL loss post-cuprizone (post-cup) administration. The images show initial loss of EGFP$^+$ myelin sheaths and subsequent shrinking of cell body before loss of the EGFP signal in a *MOBP–EGFP* mouse. **e**, Myelin loss ($n_{mice} = 3$, $n_{cells} = 45$) occurs earlier than OL soma loss ($n_{mice} = 3$, $n_{cells} = 47$; Student's *t*-test, $t(90) = -5$, $^{***}P < 0.0001$; box plots represent the median and interquartile range (IQR)). **f**, Cumulative OL gain and loss relative to baseline (percentage); traces represent individual mice. **g**, Cumulative OL loss is tightly related to OL gain (Spearman's $\rho = 0.922$, $^{***}P < 0.0001$). **h**, There is a delayed inflection point for OL replacement relative to loss (8.71 ± 0.72 versus 4.51 ± 0.68 days post-cuprizone, respectively; $n_{mice} = 5$; $t(8) = 4.24$, $^{**}P = 0.0028$; Student's *t*-test) and a decreased asymptote of replacement relative to loss (60.52 ± 3.03% versus 87.06 ± 3.10%, respectively; $t(8) = 6.12$, $^{***}P = 0.0003$; Student's *t*-test). **i**, Representative heatmaps of neuronal firing rate (FR) in the motor cortex of healthy mice (left, control) versus remyelinating mice (right, cuprizone). **j**, Neuronal FRs were comparable between control and cuprizone mice both before and during cuprizone administration, but elevated in cuprizone-treated mice both in the first and second week following cuprizone cessation (Wilcoxon rank-sum; $^{**}P = 0.0063$ and $^{*}P = 0.0157$, respectively; points represent individual neurons, lines and error bars represent the median and IQR). By 3 weeks post-cuprizone, the FRs were indistinguishable between cuprizone-treated and control mice. $^{*}P < 0.05$, $^{**}P < 0.01$, $^{***}P < 0.001$. For detailed statistics, see Supplementary Table 2, tab 3.

in healthy mice (Figs. 1 and 2), we sought to examine whether it could enhance oligodendrocyte replacement in demyelinated mice. We allotted mice to one of three experimental groups: 'no activity,' 'early learning' (starting 3 days post-cuprizone) and 'delayed learning' (starting 10 days post-cuprizone; Fig. 5a,b). Behavioral intervention did not affect the severity of demyelination (Fig. 5c) or the maximum rate of oligodendrogenesis during remyelination (Fig. 5d).

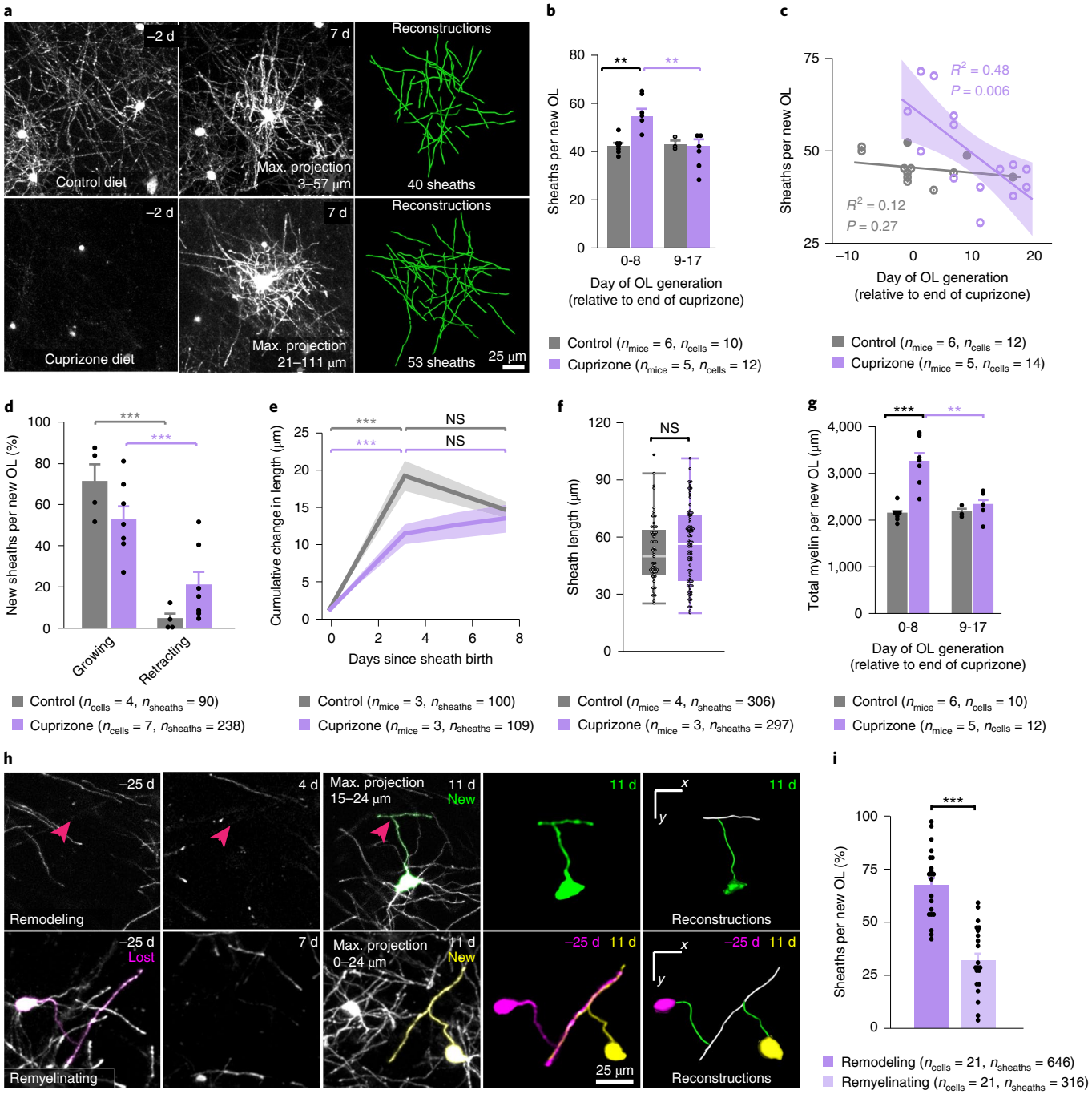

Fig. 4 | Myelin sheath numbers on new oligodendrocytes are regulated during remyelination. a,**b**, Representative images (**a**) and quantification (**b**) of remyelination modulating sheath number ($F_{1,19}$ = 8.03, P = 0.0105). OLs generated in the first week of remyelination (top, **a**) generate more sheaths than age-matched control OLs (bottom, **a**; P = 0.010, Tukey's HSD) or than OLs formed after week 1 of remyelination (P = 0.0023). Fields of view show 2 days before OL birth and 7 days post-birth. Data points represent individual OLs. Sample sizes represent total OLs across time points. **c**, The day of OL generation relative to the end of cuprizone predicts the sheath number in demyelinated mice (R^2 = 0.48, $F_{1,12}$ = 11.16, P = 0.006; shaded area represents 95% confidence of fit; points represent OLs). **d**, In the first 3 days post-generation, sheaths from new OLs grow more often than they retract ($F_{3,18}$ = 15.34, ***P < 0.0001) in both control (P = 0.0001, n_{mice} = 4) and cuprizone-treated mice (P = 0.0096, n_{mice} = 6, Tukey's HSD). Data points represent individual OLs. **e**, New sheaths change in length in the week following their generation (control: $F_{3,302}$ = 47.94, ***P < 0.0001, cuprizone: $F_{3,293}$ = 29.71, ***P < 0.0001; lines and shaded area represent the mean ± s.e.m., respectively). Sheaths in both control and cuprizone-treated mice stabilize their length within 3 days of sheath birth (day 0 versus day 3, ***P < 0.0001 in both treatments; Tukey's HSD). **f**, Sheath length does not differ between control and cuprizone-treated mice 3 days after sheath generation (boxplots represent the median and IQR; points represent sheaths). **g**, Remyelination shapes the predicted total myelin ((mean sheath length) × (no. of sheaths/OL)) generated by a new OL ($F_{1,19}$ = 8.93, P = 0.0077). It is higher in week 1 of remyelination than age-matched control OLs (***P < 0.0001) or than OLs generated after week 1 of remyelination (P = 0.0016; Tukey's HSD). **h**, New OLs can place sheaths in previously unmyelinated areas (top, 'Remodeling') or previously myelinated areas (bottom, 'Remyelinating'). Pink arrowheads indicate junctions between a new sheath and a new OL process. Relevant sheaths are pseudocolored. **i**, New OLs engage in remodeling more often than remyelinating (t(20) = −5.08, ***P < 0.0001, n_{mice} = 5; paired Student's t-test). *P < 0.05, **P < 0.01, ***P < 0.001; bars and error bars represent the mean ± s.e.m. For detailed statistics, see Supplementary Table 2, tab 4.

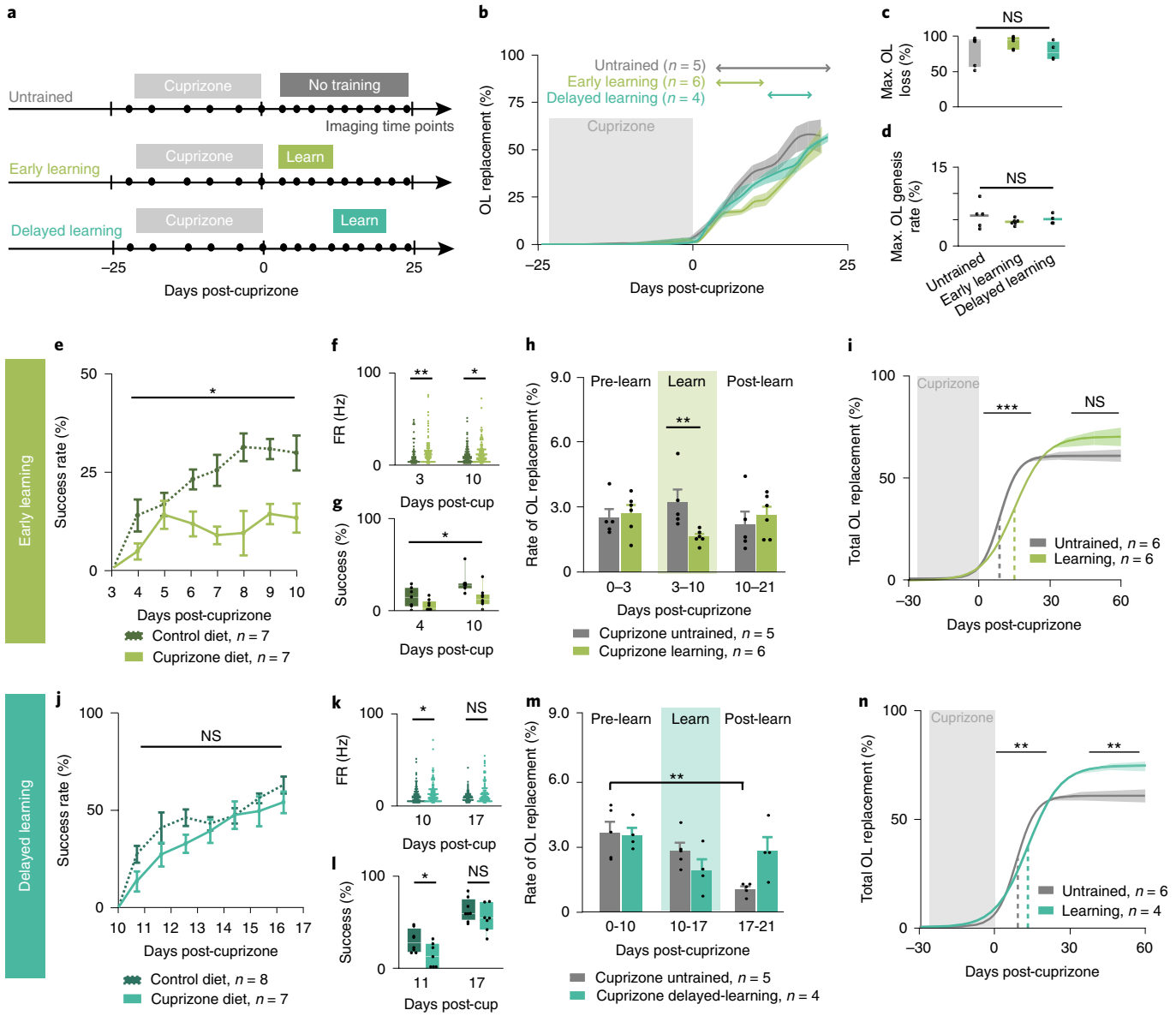

Fig. 5 | Motor learning modulates oligodendrogenesis after demyelination in a timing-dependent manner. a,**b**, Schematic of the protocol (**a**) and cumulative OL replacement (**b**; percentage; lines and shaded areas represent the mean ± s.e.m., respectively) across post-cuprizone behavioral interventions. **c**,**d**, Neither maximum OL loss (**c**) nor maximum rate of oligodendrogenesis (**d**) differ between behavioral interventions (boxplots represent the median and IQR). **e**, Demyelination modulates early-learning success rate ($F_{6,78} = 3.00$, $P = 0.011$; points represent the mean ± s.e.m.). Success rate improves from the first to the last day of reaching for control mice ($P = 0.005$; Tukey's HSD), but not for cuprizone-treated mice. **f**, Both 3 and 10 days post-cuprizone, demyelinated mice have increased neuronal FRs relative to controls (Wilcoxon rank-sum, $P = 0.006$ and $P = 0.016$, respectively; points represent neurons). **g**, Both 4 and 10 days post-cuprizone, demyelinated mice have decreased success rates relative to controls ($F_{1,13} = 9.09$, $P = 0.01$; points represent mice). **h**, OL replacement rate is suppressed during early learning relative to untrained demyelinated mice (Wilcoxon rank-sum, $P = 0.0043$). **i**, There is a delayed inflection point (indicated by broken vertical lines) of OL replacement in early-learning versus untrained demyelinated mice (Student's *t*-test; $t(10) = 5.77$, $P = 0.0002$; colored line and shaded area represents the asymptote ± s.e.m., respectively). **j**, There is no effect of cuprizone treatment on overall delayed-learning performance. **k**, At 10 days post-cuprizone, but not 17 days post-cuprizone, demyelinated mice have increased neuronal FRs relative to controls (Wilcoxon rank-sum, $P = 0.016$). **l**, At 11 days post-cuprizone, but not 17 days post-cuprizone, demyelinated mice have impaired reaching performance relative to controls (Student's *t*-test; $t(12.28) = -2.39$, $P = 0.033$). **m**, Delayed learning modulates OL replacement rate ($F_{2,14} = 4.61$, $P = 0.029$). Rate decreases in untrained, but not delayed-learning, mice by 21 days post-cuprizone ($P = 0.008$; Tukey's HSD). **n**, There is a delayed inflection point (Student's *t*-test; $t(8) = 4.33$, $P = 0.0025$) and increased asymptote of OL replacement ($t(8) = 3.35$, $P = 0.01$) in delayed-learning versus untrained mice. $^*P < 0.05$, $^{**}P < 0.01$, $^{***}P < 0.001$; bars and error bars represent the mean ± s.e.m. For detailed statistics, see Supplementary Table 2, tab 5.

Mice in the early-learning group showed significant performance impairments relative to healthy controls and did not improve their reaching across the learning period, which indicates that there is a failure to acquire the reach task (Fig. 5e; Extended Data Fig. 6). While cuprizone did not alter the number of overall reach attempts, the extent of demyelination was negatively related to performance (Extended Data Fig. 6). Motor deficits were temporally correlated to neuronal hyperexcitability in the forelimb region of the motor cortex, whereby the firing rate was increased in demyelinated versus healthy mice in the first 10 days post-cuprizone, which coincided

with the entire early-learning period (Fig. 5f,g). Learning suppressed oligodendrocyte replacement rate by approximately 50% relative to untrained remyelinating mice (1.62 ± 0.13% versus 3.21 ± 0.59%, respectively; Fig. 5b,h), resulting in a delayed inflection point of oligodendrocyte replacement (15 versus 9 days post-cuprizone, respectively; Fig. 5i). However, the asymptote of oligodendrogenesis did not differ between untrained and early-learning mice. The learning-induced suppression was less severe in remyelinating mice than in healthy controls (50 versus 75%, respectively; Fig. 1) and we did not observe an increase in oligodendrogenesis rate post-training (Fig. 5h). Success during learning was unrelated to the asymptote of oligodendrocyte replacement among the mice (Extended Data Fig. 6). In sum, motor performance was impaired and motor cortex neurons were hyperexcitable following demyelination, and failing to learn the reach task provided no benefit to oligodendrogenesis during remyelination.

Since mice that were trained immediately following cuprizone cessation were unable to learn, we trained mice 10 days post-cuprizone (that is, the half-maximum of the remyelination response; Fig. 3h). These delayed-learning mice did not show overall impairments in reaching performance (Fig. 5j) or reaching attempts (Extended Data Fig. 6) relative to healthy mice. Again, we found that neuronal hyperexcitability was temporally correlated to reaching success. While demyelinated mice were slightly less successful than healthy controls on the initial day of training (10 days post-cuprizone, when demyelinated mice still show motor cortex neuronal hyperexcitability; Fig. 5k,l), their success rates were indistinguishable from controls by the end of training (17 days post-cuprizone). Delayed learners demonstrated a slight decrease in oligodendrogenesis rate during learning (~30%) that was not significantly different from untrained demyelinated mice (Fig. 5b,m). While the rate of oligodendrogenesis slowed by 3 weeks post-cuprizone in untrained mice, it did not in delayed learners. The inflection point of oligodendrocyte replacement was therefore delayed in delayed learners (13 versus 9 days post-cuprizone, respectively; Fig. 5n), and oligodendrocyte replacement plateaued substantially higher than in untrained mice (74.56 ± 2.26% versus 60.52 ± 3.03%, respectively). Success during delayed learning was not related to oligodendrocyte replacement (Extended Data Fig. 6). In sum, partial remyelination restored both neuronal function and the ability to learn the forelimb reach task, and motor learning following partial remyelination promoted long-term oligodendrogenesis.

To control for motor activity rather than motor learning, mice were trained pre-cuprizone administration and rehearsed the forelimb reach task post-cuprizone treatment (Extended Data Fig. 7). Although demyelinated mice demonstrated performance deficits during rehearsal, rehearsal did not modulate any aspect of remyelination. Only learning the reach task (delayed learning), but not attempting to learn it (early learning) or rehearsing it (rehearsal), promoted oligodendrogenesis post-cuprizone treatment.

By 7 weeks post-cuprizone, delayed-learning mice replaced over 20% more oligodendrocytes and had over 40% greater density of oligodendrocytes in layers I–III of the motor cortex than age-matched, demyelinated, untrained mice (79.24 ± 4.56% versus 58.43 ± 5.26%, and 86.67 ± 5.36 versus 60.67 ± 4.06 oligodendrocytes per 0.06 mm^3, respectively; Fig. 6a–c). Delayed learning did not modulate the number of sheaths per new oligodendrocyte (Fig. 6d), but did increase the proportion of sheaths that retracted over time (Fig. 6e), which is similar to the observations in healthy mice (Fig. 1i–k). Sheaths from new oligodendrocytes were equally likely to remyelinate denuded axons in both untrained and delayed-learning mice (Fig. 6f). Using the 'mean sheath number per new oligodendrocyte per mouse' parameter, we modeled the restoration of baseline sheath number and remyelination of denuded axons to the population level. While untrained and delayed-learning mice replaced similar proportions of baseline sheath number before behavioral intervention (19.59 ± 0.97% and 24.05 ± 6.54%, respectively; Fig. 6g), delayed learners replaced almost twice as many lost sheaths as untrained mice post-training (62.22 ± 8.12% versus 34.72 ± 8.84%) due to prolonged oligodendrogenesis (Figs. 5n and 6a–c). As a result, we project that by 7 weeks post-cuprizone, delayed learners would have replaced almost 90% of their baseline sheath number, versus only 54% in untrained mice (Fig. 6h). Increased sheath generation by delayed learners resulted in a predicted twofold increase in remyelination of denuded axons relative to untrained mice (30.19 ± 1.33% versus 16.38 ± 2.37%, respectively; Fig. 6i).

Motor learning promotes the participation of preexisting mature oligodendrocytes in remyelination. To determine the contribution of preexisting mature oligodendrocytes to remyelination, we used longitudinal in vivo imaging and semiautomated tracing[20] to reconstruct myelin sheaths and connecting processes to the oligodendrocyte cell body (Extended Data Fig. 2). We then tracked myelin sheaths of individual oligodendrocytes throughout cuprizone-mediated demyelination and remyelination (Extended Data Fig. 8; see Methods). Oligodendrocyte survival was variable between mice, but did not differ in untrained and delayed-learning groups (12.29 ± 7.32% versus 20.84 ± 6.60%; Extended Data Fig. 8). After 3 weeks of cuprizone treatment in untrained mice, all surviving oligodendrocytes experienced sheath loss, and in rare instances (1 out of 19) oligodendrocytes added a new sheath (Fig. 7a–d; Supplementary Videos 12 and 13). While preexisting myelin sheaths in healthy mice rarely remodeled (Fig. 1), cuprizone treatment increased preexisting sheath retraction in surviving oligodendrocytes (17.0 ± 4.22% versus 43.8 ± 5.95%; Extended Data Fig. 9). Delayed learning did not affect the degree of remodeling in preexisting myelin sheaths during remyelination (Extended Data Fig. 9), but dramatically increased the number of preexisting oligodendrocytes that generated new myelin sheaths (Fig. 7d,e). Sheath generation in preexisting oligodendrocytes followed a similar time course to new oligodendrocytes, with sheaths growing during the first 3 days post-generation before stabilization (Extended Data Fig. 9). In healthy mice, preexisting oligodendrocytes were never observed to generate new sheaths (Extended Data Fig. 9); however, in delayed-learning mice, preexisting oligodendrocytes were able to generate sheaths even 1.7 months after the onset of imaging, which suggests that the ability to generate myelin sheaths is an extended property of oligodendrocytes (Fig. 7f).

The generation of new sheaths from preexisting oligodendrocytes was temporally correlated to the onset of forelimb reach training. The number of preexisting oligodendrocytes generating new sheaths increased by over 40% during learning and persisted in the subsequent weeks (Fig. 7g; Supplementary Videos 13 and 14). As such, delayed learners had a higher cumulative number of new sheaths generated by surviving oligodendrocytes than untrained mice both during and after learning (Fig. 7h). Myelin sheath loss stagnated in surviving oligodendrocytes after the onset of learning, which was in contrast to sheath loss in untrained mice, which continued for 2 weeks post-cuprizone (Fig. 7i). The number of lost myelin sheaths was unrelated to sheaths generated on individual oligodendrocytes (Fig. 7j).

As with oligodendrogenesis following learning, sheath addition by preexisting oligodendrocytes was higher in layer I versus layer II/III of the cortex (Fig. 7k,l; Supplementary Video 15). Surviving oligodendrocytes formed new myelin sheaths on both denuded and previously unmyelinated axons (Fig. 7m; Supplementary Videos 16 and 17). A significantly larger proportion of surviving oligodendrocyte sheaths remyelinated denuded axons relative to newly generated oligodendrocytes (Fig. 7n). The combination of learning-induced cessation of sheath loss and new sheath generation from surviving oligodendrocytes resulted in a greater

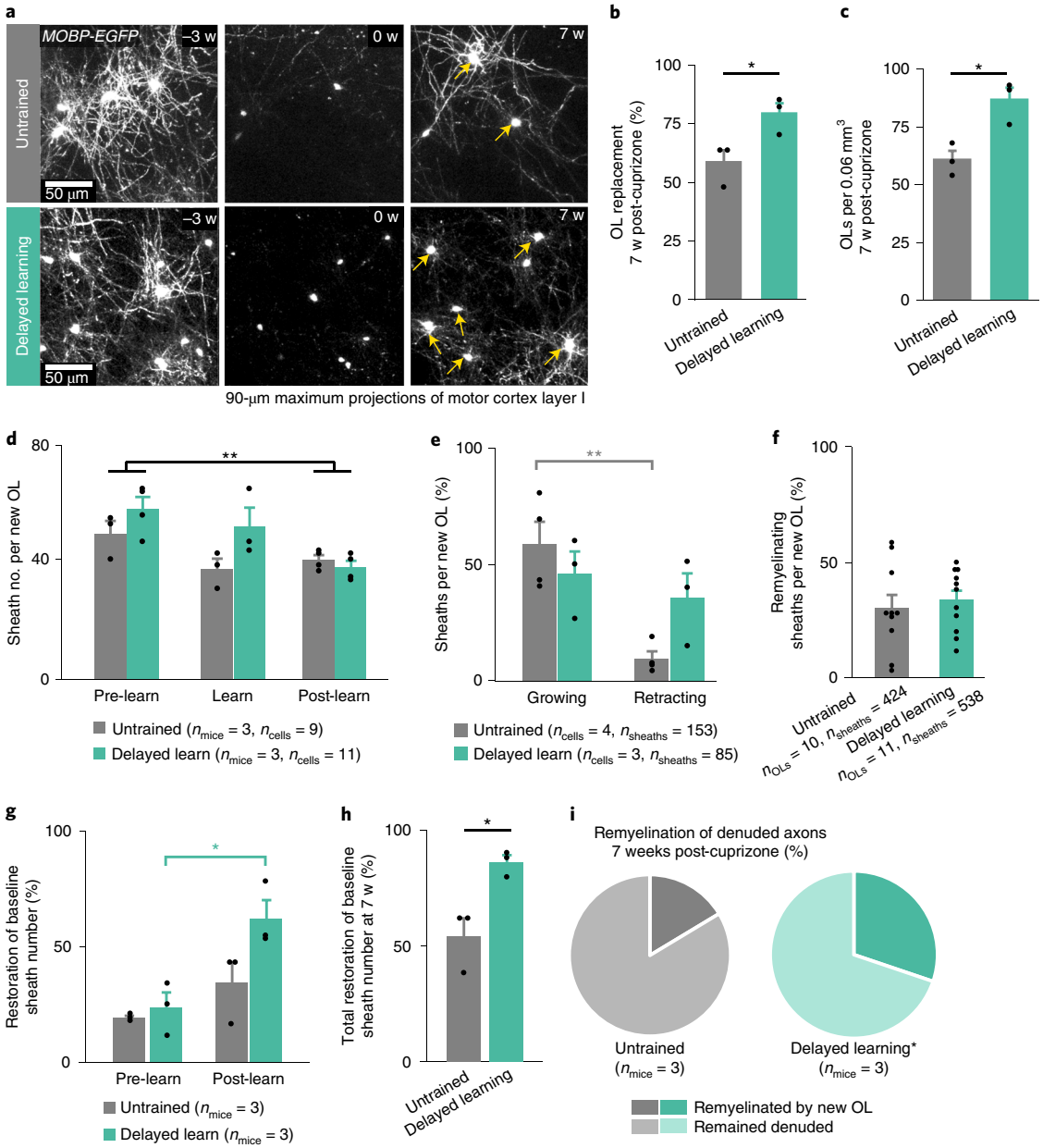

Fig. 6 | Delayed motor learning promotes remyelination via new oligodendrocytes. a, Representative maximum projections of superficial cortical OLs (0–90 µm) at baseline (left; −3 weeks), at the end of the cuprizone diet (middle; 0 weeks) and following 7 weeks of remyelination (right) in untrained (top) and delayed-learning (bottom) mice. Yellow arrows designate new OLs. **b**,**c**, Delayed learners replace a greater proportion of lost OLs (**b**; Student's *t*-test; $t(3.92) = -2.99$, $P = 0.04$) and have a higher density of cortical OLs than untrained mice (**c**; $t(3.72) = -3.87$, $P = 0.02$) by 7-weeks post-cuprizone (points represent individual mice). **d**, While new OLs have increased sheath numbers in the first versus the third week post-cuprizone treatment ($F_{5,15} = 5.14$, $P = 0.006$; $P = 0.0038$, Tukey's HSD), delayed learning does not modulate this relationship ($P = 0.1$; points represent individual OLs.) **e**, Delayed learning modulates sheath dynamics ($F_{3,10} = 6.65$, $P = 0.0095$). Sheaths on new OLs are more likely to grow than retract in untrained mice ($P = 0.007$, Tukey's HSD), but not in delayed-learning mice ($P > 0.8$; points represent individual OLs.) **f**, Sheaths from new OLs are equally likely to remyelinate denuded axons in both untrained and delayed-learning mice (Student's *t*-test; $t(16.08) = -0.52$, $P = 0.6$; points represent individual OLs). **g**, Population-level extrapolations suggest that delayed-learning modulates the restoration of the baseline sheath number ($F_{3,8} = 7.80$, $P = 0.0093$; points represent mice). More sheaths are replaced after training in delayed-learning mice (Tukey's HSD; $p = 0.018$). **h**, Population-level extrapolations suggest that delayed learners restore a greater proportion of baseline sheath number 7 weeks post-cuprizone (Student's *t*-test; $t(2.64) = -3.76$, $P = 0.0407$; points represent mice). **i**, Extrapolating the sheath location probability to the population-level suggests that delayed learners remyelinate a greater proportion of denuded axons than untrained mice (31% versus 19%, respectively; Student's *t*-test; $t(3.14) = -5.07$, $P = 0.013$). $^*P < 0.05$, $^{**}P < 0.01$, $^{***}P < 0.001$; bars and error bars represent the mean ± s.e.m. For detailed statistics, see Supplementary Table 2, tab 6.

maintenance of the original myelination pattern in delayed-learning mice relative to untrained mice (Fig. 7o). Preexisting oligodendrocytes engaging in new myelin sheath deposition showed an increase in overall cell body volume of 141 ± 15% (Extended Data Fig. 10). These findings indicate that following demyelination, motor learning specifically enhances the ability of preexisting oligodendrocytes to generate additional myelin and to maintain preexisting sheaths (Supplementary Fig. 1).

Discussion

Tissue regeneration following injury or disease is a long sought-after goal, particularly in the adult nervous system. Oligodendroglia represent one of the few cell types that retain the capacity to regenerate and repair following damage to the adult CNS. Remyelination of denuded axons can restore neuronal function[3], promote neuroprotection[29] and may facilitate functional recovery in CNS diseases characterized by myelin loss[6].

In this study, we showed that learning shapes the pattern of myelination in the healthy and remyelinating brain. Longitudinal in vivo two-photon imaging of the forelimb motor cortex throughout the learning of a forelimb reach task revealed that learning transiently suppressed oligodendrogenesis but subsequently increased oligodendrocyte generation, OPC differentiation and retraction of preexisting myelin sheaths. Cuprizone-mediated demyelination induced ~90% of oligodendrocyte loss and neuronal firing rate abnormalities in the forelimb region of the motor cortex, as well as deficits in motor performance. Motor learning only occurred following the partial remyelination and restoration of neuronal function, and resulted in greater oligodendrocyte and myelin sheath replacement. Additionally, motor learning enhanced the ability of surviving oligodendrocytes to participate in remyelination via the generation of new sheaths. These results demonstrate that motor learning can improve remyelination via cortical oligodendrogenesis and myelin sheath formation by surviving oligodendrocytes (Supplementary Fig. 1).

To our knowledge, we are the first to observe transient learning-induced suppression in oligodendrocyte generation. OPC differentiation was unaffected during this suppression, which suggests that learning may temporarily decrease the survival and integration of differentiated OPCs as mature myelinating oligodendrocytes, which is in line with previous work in the developing CNS[30]. These nuanced effects may be apparent due to our high intraindividual resolution and regional specificity, whereas previous studies have not parcellated the motor cortex based on function[17]. It is possible that location-specific cues suppress the integration of new oligodendrocytes to prevent aberrant myelination during learning or that metabolic demand imposed by network plasticity during learning[31] may deplete the resources required for the generation and integration of adjacent oligodendrocytes[32]. How these learning-induced changes are communicated to the oligodendrocyte lineage cells remains undefined. Axons form synapses with local OPCs, and neuronal activity can modulate OPC proliferation and differentiation within both the healthy CNS and demyelinated regions[16,33]. This communication may be mediated by the effects of brain-derived neurotrophic factor on both activity-dependent synaptic modulation and oligodendrocyte maturation and myelination[34]. Future work characterizing the mechanisms underlying activity-dependent oligodendrogenesis, particularly during different life stages, will provide additional insight into the promotion of recovery from demyelinating injury.

We previously reported that environmental enrichment increases oligodendrogenesis but not myelin sheath remodeling in the somatosensory cortex of middle-aged mice[19]; however, here, we found that motor learning increased both oligodendrogenesis and myelin sheath remodeling in the motor cortex of young adult mice. This disparity may be due to heterogeneity[35], regional variance between somatosensory and motor oligodendrocytes or age-related decreases in remodeling capacity, as is observed with synaptic plasticity[36]. The role of sheath retraction throughout learning remains to be explored, although recent work suggests that this may regulate conduction velocity[37] and potentially allow for increased axonal branching or synapse formation. Concurrent multicolor in vivo imaging of reach-related neurons and myelin sheaths throughout learning will clarify how neurons and oligodendrocytes interact during circuit consolidation.

The consequences of demyelination on the function of intact cortical neural circuits is not well understood. We found that neural firing rates increased following demyelination, and resulted in hyperexcitability of the forelimb motor cortex. Despite effects of copper chelation on NMDA and AMPA receptor currents and neuronal excitability[38], cuprizone treatment did not affect concurrent neuronal firing rates in vivo, findings that are similar to previous accounts of ex vivo whole-cell recordings[28]. Hyperexcitability is a common feature of neurodegenerative diseases and can be a consequence of increased cellular stressors, including elevated intracellular calcium load[39] as is observed in experimental autoimmune encephalomyelitis models of MS[40]. The accumulation of cellular stress as a result of demyelination may be a potential cause of the neurodegeneration seen in patients with progressive MS. In addition to cell-autonomous mechanisms, hyperexcitability may also result from changes in the complex excitatory and inhibitory balance within the motor cortex control of movement, for example, via alterations in the myelination of thalamocortical input, corticospinal output axons or local circuitry. In neurodegenerative disorders, local circuit processing alterations produce hyperexcitability[41], which predicts motor impairments in both human patients and animal models[42,43]. We found that neuronal activity in remyelinating mice was indistinguishable from healthy controls when superficial motor cortex remyelination plateaued, and that this partial remyelination rescued motor deficits. These data show a clear link between cortical myelin content, neuronal function and motor

Fig. 7 | Delayed motor learning stimulates surviving mature oligodendrocytes to contribute to remyelination. a, Identification of surviving OLs via process morphology. Note the new process on the same OL in **a** and **c** (cyan arrowhead). **b**–**d**, Surviving OLs in untrained mice and delayed-learning mice both lose (**b**, pink) and generate sheaths (**c**, green). Additional *z*-planes were included in the maximum projection in **c** (44 days) to show the sheath and the process connecting to the cell body. Quantification shown in **d**. **e**, Number of sheaths generated per surviving OL. **f**, Minimum possible OL age at time of sheath generation (assuming age 0 at imaging onset). **g**, Delayed learning modulates surviving OL sheath production ($F_{2,51} = 9.30$, $P = 0.0004$). Sheath generation increases during learning (***$P < 0.0001$) and decreases post-learning ($P = 0.019$), resulting in an elevated generation relative to untrained mice both during (***$P < 0.0001$) and after learning ($P = 0.026$). **h**, Learning modulates cumulative new sheaths on surviving OLs ($F_{7,618} = 12.96$, ***$P < 0.0001$). Delayed learning increases new sheaths relative to baseline ($P = 0.019$) and relative to untrained mice both during ($P = 0.028$) and after ($P = 0.033$) learning. The sheath number increases up to 4 weeks post-learning (***$P < 0.0001$). **i**, Learning modulates the cumulative number of lost sheaths on surviving OLs ($F_{7,611} = 7.04$, ***$P < 0.0001$). Sheath loss initially increases in untrained and delayed-learning mice (***$P < 0.0001$ and ***$P < 0.0001$, respectively), and then ceases in delayed-learning ($P > 0.9$) but not untrained mice (***$P < 0.0001$). **j**, There is no relationship between sheath loss and gain ([a]note that a single outlier was removed for analysis). **k**,**l**, Learning increases sheath generation by surviving OLs in both layers I and III relative to controls ($F_{1,6} = 7.05$, $P = 0.038$; $P = 0.0019$ and $P = 0.0016$, respectively), though generation is heightened within layer I versus layer II/III ($P = 0.044$). Pink arrows indicate junction between new sheath and surviving OL process. Relevant sheaths are pseudocolored. **m**,**n**, Three weeks post-cuprizone, new sheaths from surviving OLs are more likely to remyelinate denuded axons than sheaths from new OLs ($t(2) = 7.28$, $P = 0.018$). **o**, Surviving OLs in delayed-learning mice contribute more sheaths to the original pattern of myelination (via maintenance and addition) than untrained mice ($t(35) = -2.25$, $P = 0.031$). *$P < 0.05$, **$P < 0.01$, **$P < 0.001$, bars and error bars represent the mean ± s.e.m. For statistics, see Supplementary Table 2, tab 7.

behavior. Future work characterizing the cell-type-specific changes in neuronal excitability[44] and plasticity[45], along with circuit-level alterations in excitatory and inhibitory balance within the motor cortex[46], will provide insights into the cellular and circuit origins of demyelination-induced hyperexcitability.

Recent analyses of tissue from patients with MS suggest that shadow plaques are incompletely demyelinated lesions or lesions remyelinated by preexisting oligodendrocytes[7,8]. Our data clearly demonstrate that both scenarios occur following demyelination. Furthermore, we showed that the remyelinating potential of

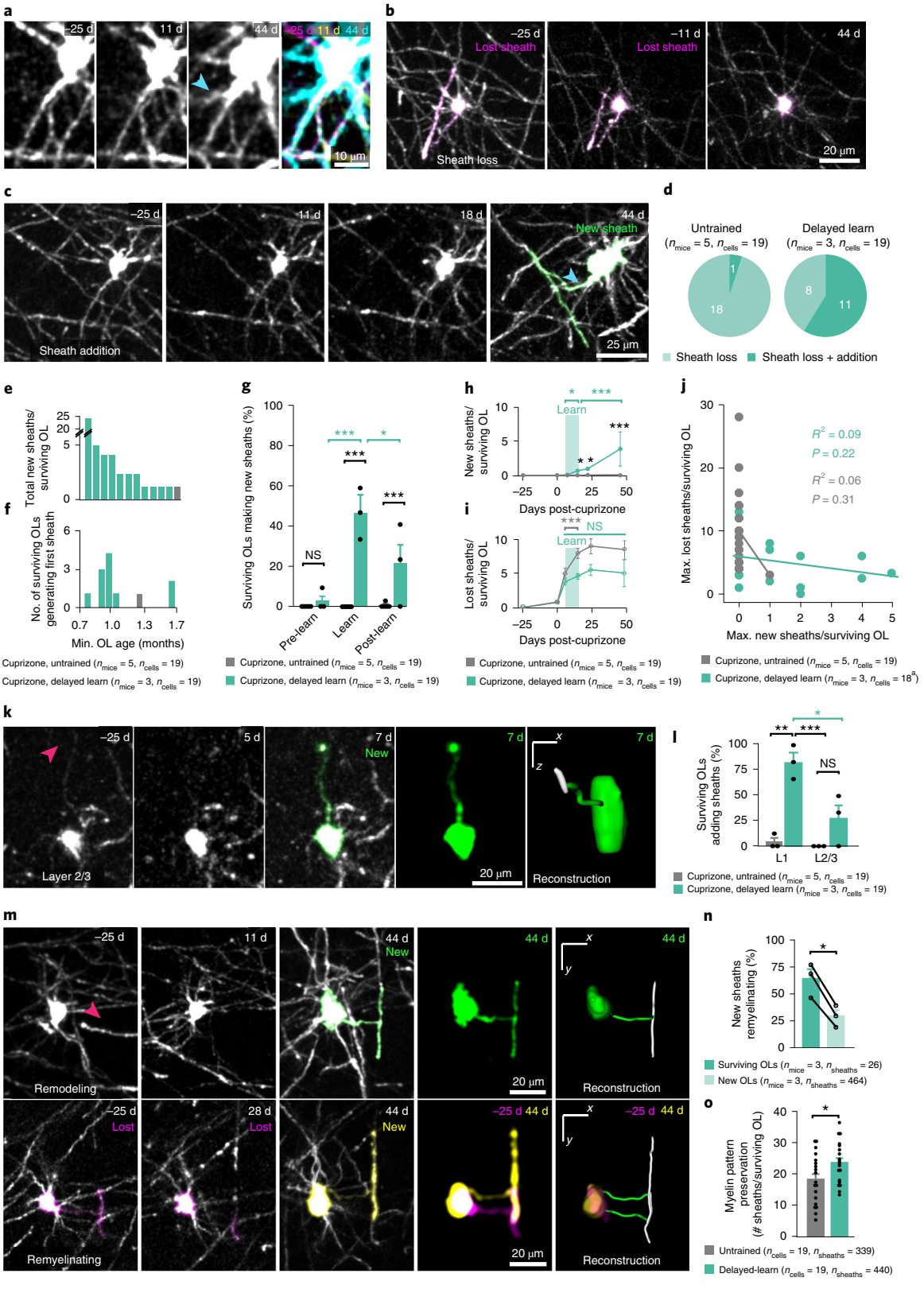

preexisting mature oligodendrocytes is modulated by learning. While the majority of surviving oligodendrocytes contributed new myelin sheaths following learning, the variability in magnitude of this response raises questions about what drives certain oligodendrocytes to generate more myelin than others. Proximity to a learning-relevant neural circuit may modulate the amount of new myelin deposited by surviving oligodendrocytes[47,48]. Exploring whether surviving oligodendrocytes preferentially myelinate axons that they are already ensheathing may provide insight into whether direct axo–myelinic communication[49] plays a role in initiating the remyelination response in preexisting oligodendrocytes. Continued reductions in cell soma size and progressive compaction of chromatin are hallmarks of OPC maturation into myelinating oligodendrocytes[50,51]. The increase in cell soma volume during surviving oligodendrocyte remyelination suggests that epigenetic regulation of gene expression may regulate the generation of new myelin, which is similar to recent findings in tissue samples from patients with MS[7]. The identification of gene expression changes in mature oligodendrocytes engaging in new sheath deposition could provide insight into the molecular mechanisms driving remyelination by mature oligodendrocytes and provide new therapeutic targets to promote remyelination.

Behavioral interventions used to support motor function in patients with MS[14] may also engage endogenous mechanisms to stimulate myelin addition after injury. Notably, motor learning implemented after the onset of remyelination prolonged the duration of oligodendrogenesis, increased oligodendrocyte replacement, nearly restored baseline sheath number and promoted the remyelination of denuded axons by both new and surviving oligodendrocytes. Overall, our findings argue that specifically timed therapeutic interventions designed to promote oligodendrogenesis and to engage mature oligodendrocytes in myelin repair may enhance remyelination and accelerate functional recovery in demyelinating disorders.

Online content

Any methods, additional references, Nature Research reporting summaries, source data, extended data, supplementary information, acknowledgements, peer review information; details of author contributions and competing interests; and statements of data and code availability are available at https://doi.org/10.1038/s41593-020-0637-3.

Received: 10 May 2019; Accepted: 7 April 2020;
Published online: 18 May 2020

References

1. Reich, D. S., Lucchinetti, C. F. & Calabresi, P. A. Multiple sclerosis. *N. Engl. J. Med.* **378**, 169–180 (2018).
2. Hauser, S. L., Chan, J. R. & Oksenberg, J. R. Multiple sclerosis: prospects and promise. *Ann. Neurol.* **74**, 317–327 (2013).
3. Périer, O. & Grégoire, A. Electron microscopic features of multiple sclerosis lesions. *Brain* **88**, 937–952 (1965).
4. Tripathi, R. B., Rivers, L. E., Young, K. M., Jamen, F. & Richardson, W. D. NG2 glia generate new oligodendrocytes but few astrocytes in a murine experimental autoimmune encephalomyelitis model of demyelinating disease. *J. Neurosci.* **30**, 16383–16390 (2010).
5. Prineas, J. W. & Connell, F. Remyelination in multiple sclerosis. *Ann. Neurol.* **5**, 22–31 (1979).
6. Green, A. J. et al. Clemastine fumarate as a remyelinating therapy for multiple sclerosis (ReBUILD): a randomised, controlled, double-blind, crossover trial. *Lancet* **390**, 2481–2489 (2017).
7. Jäkel, S. et al. Altered human oligodendrocyte heterogeneity in multiple sclerosis. *Nature* **566**, 543–547 (2019).
8. Yeung, M. S. Y. et al. Dynamics of oligodendrocyte generation in multiple sclerosis. *Nature* **566**, 538–542 (2019).
9. Crawford, A. H. et al. Pre-existing mature oligodendrocytes do not contribute to remyelination following toxin-induced spinal cord demyelination. *Am. J. Pathol.* **186**, 511–516 (2016).
10. Duncan, I. D. et al. The adult oligodendrocyte can participate in remyelination. *Proc. Natl Acad. Sci. USA* **115**, E11807–E11816 (2018).
11. Hughes, E. G. & Appel, B. The cell biology of CNS myelination. *Curr. Opin. Neurobiol.* **39**, 93–100 (2016).
12. Scholz, J., Klein, M. C., Behrens, T. E. J. & Johansen-Berg, H. Training induces changes in white-matter architecture. *Nat. Neurosci.* **12**, 1370–1371 (2009).
13. Sampaio-Baptista, C. et al. Motor skill learning induces changes in white matter microstructure and myelination. *J. Neurosci.* **33**, 19499–19503 (2013).
14. Beer, S., Khan, F. & Kesselring, J. Rehabilitation interventions in multiple sclerosis: an overview. *J. Neurol.* **259**, 1994–2008 (2012).
15. Albert, M., Antel, J., Brück, W. & Stadelmann, C. Extensive cortical remyelination in patients with chronic multiple sclerosis. *Brain Pathol.* **17**, 129–138 (2007).
16. Gibson, E. M. et al. Neuronal activity promotes oligodendrogenesis and adaptive myelination in the mammalian brain. *Science* **344**, 1252304 (2014).
17. McKenzie, I. A. et al. Motor skill learning requires active central myelination. *Science* **346**, 318–322 (2014).
18. Xu, T. et al. Rapid formation and selective stabilization of synapses for enduring motor memories. *Nature* **462**, 915–919 (2009).
19. Hughes, E. G., Orthmann-Murphy, J. L., Langseth, A. J. & Bergles, D. E. Myelin remodeling through experience-dependent oligodendrogenesis in the adult somatosensory cortex. *Nat. Neurosci.* **21**, 696–706 (2018).
20. Longair, M. H., Baker, D. A. & Armstrong, J. D. Simple neurite tracer: open source software for reconstruction, visualization and analysis of neuronal processes. *Bioinformatics* **27**, 2453–2454 (2011).
21. Harms, K. J., Rioult-Pedotti, M. S., Carter, D. R. & Dunaevsky, A. Transient spine expansion and learning-induced plasticity in layer 1 primary motor cortex. *J. Neurosci.* **28**, 5686–5690 (2008).
22. Hill, R. A., Li, A. M. & Grutzendler, J. Lifelong cortical myelin plasticity and age-related degeneration in the live mammalian brain. *Nat. Neurosci.* **21**, 683–695 (2018).
23. Hughes, E. G., Kang, S. H., Fukaya, M. & Bergles, D. E. Oligodendrocyte progenitors balance growth with self-repulsion to achieve homeostasis in the adult brain. *Nat. Neurosci.* **16**, 668–676 (2013).
24. Franklin, R. J. M. & ffrench-Constant, C. Regenerating CNS myelin—from mechanisms to experimental medicines. *Nat. Rev. Neurosci.* **18**, 753–769 (2017).
25. Baxi, E. G. et al. Lineage tracing reveals dynamic changes in oligodendrocyte precursor cells following cuprizone-induced demyelination. *Glia* **65**, 2087–2098 (2017).
26. Johnson, E. S. & Ludwin, S. K. Evidence for a 'dying-back' gliopathy in demyelinating disease. *Ann. Neurol.* **9**, 301–305 (1981).
27. Buzsáki, G. Large-scale recording of neuronal ensembles. *Nat. Neurosci.* **7**, 446–451 (2004).
28. Hamada, M. S. & Kole, M. H. P. Myelin loss and axonal ion channel adaptations associated with gray matter neuronal hyperexcitability. *J. Neurosci.* **35**, 7272–7286 (2015).
29. Mei, F. et al. Accelerated remyelination during inflammatory demyelination prevents axonal loss and improves functional recovery. *eLife* **5**, e18246 (2016).
30. Hill, R. A., Patel, K. D., Goncalves, C. M., Grutzendler, J. & Nishiyama, A. Modulation of oligodendrocyte generation during a critical temporal window after NG2 cell division. *Nat. Neurosci.* **17**, 1518–1527 (2014).
31. Picard, N., Matsuzaka, Y. & Strick, P. L. Extended practice of a motor skill is associated with reduced metabolic activity in M1. *Nat. Neurosci.* **16**, 1340–1347 (2013).
32. Harris, J. J. & Attwell, D. The energetics of CNS white matter. *J. Neurosci.* **32**, 356–371 (2012).
33. Ortiz, F. C. et al. Neuronal activity in vivo enhances functional myelin repair. *JCI Insight* **4**, e123434 (2019).
34. Geraghty, A. C. et al. Loss of adaptive myelination contributes to methotrexate chemotherapy-related cognitive impairment. *Neuron* **103**, 250–265.e8 (2019).
35. Marques, S. et al. Oligodendrocyte heterogeneity in the mouse juvenile and adult central nervous system. *Science* **352**, 1326–1329 (2016).
36. Burke, S. N. & Barnes, C. A. Neural plasticity in the ageing brain. *Nat. Rev. Neurosci.* **7**, 30–40 (2006).
37. Ford, M. C. et al. Tuning of Ranvier node and internode properties in myelinated axons to adjust action potential timing. *Nat. Commun.* **6**, 8073 (2015).
38. You, H. et al. Aβ neurotoxicity depends on interactions between copper ions, prion protein, and *N*-methyl-D-aspartate receptors. *Proc. Natl Acad. Sci. USA* **109**, 1737–1742 (2012).
39. Saxena, S. & Caroni, P. Selective neuronal vulnerability in neurodegenerative diseases: from stressor thresholds to degeneration. *Neuron* **71**, 35–48 (2011).
40. Witte, M. E. et al. Calcium Influx through plasma-membrane nanoruptures drives axon degeneration in a model of multiple sclerosis. *Neuron* **101**, 615–624.e5 (2019).
41. Werner, C. T., Williams, C. J., Fermelia, M. R., Lin, D.-T. & Li, Y. Circuit mechanisms of neurodegenerative diseases: a new frontier with miniature fluorescence microscopy. *Front. Neurosci.* **13**, 1174 (2019).

42. Potter, L. E. et al. Altered excitatory–inhibitory balance within somatosensory cortex is associated with enhanced plasticity and pain sensitivity in a mouse model of multiple sclerosis. *J. Neuroinflammation* **13**, 142 (2016).
43. Van den Bos, M. A. J. et al. Imbalance of cortical facilitatory and inhibitory circuits underlies hyperexcitability in ALS. *Neurology* **91**, e1669–e1676 (2018).
44. Kim, J. et al. Changes in the excitability of neocortical neurons in a mouse model of amyotrophic lateral sclerosis are not specific to corticospinal neurons and are modulated by advancing disease. *J. Neurosci.* **37**, 9037–9053 (2017).
45. Ellwardt, E. et al. Maladaptive cortical hyperactivity upon recovery from experimental autoimmune encephalomyelitis. *Nat. Neurosci.* **21**, 1392–1403 (2018).
46. Denève, S. & Machens, C. K. Efficient codes and balanced networks. *Nat. Neurosci.* **19**, 375–382 (2016).
47. Hines, J. H., Ravanelli, A. M., Schwindt, R., Scott, E. K. & Appel, B. Neuronal activity biases axon selection for myelination in vivo. *Nat. Neurosci.* **18**, 683–689 (2015).
48. Mensch, S. et al. Synaptic vesicle release regulates myelin sheath number of individual oligodendrocytes in vivo. *Nat. Neurosci.* **18**, 628–630 (2015).
49. Hughes, A. N. & Appel, B. Oligodendrocytes express synaptic proteins that modulate myelin sheath formation. *Nat. Commun.* **10**, 4125 (2019).
50. Mori, S. & Leblond, C. P. Electron microscopic identification of three classes of oligodendrocytes and a preliminary study of their proliferative activity in the corpus callosum of young rats. *J. Comp. Neurol.* **139**, 1–28 (1970).
51. Shen, S., Li, J. & Casaccia-Bonnefil, P. Histone modifications affect timing of oligodendrocyte progenitor differentiation in the developing rat brain. *J. Cell Biol.* **169**, 577–589 (2005).

Methods

Animals. All animal experiments were conducted in accordance with protocols approved by the Animal Care and Use Committee at the University of Colorado Anschutz Medical Campus. Male and female mice used in these experiments were kept on a 14-h light–10-h dark schedule with ad libitum access to food and water, aside from training-related food restriction (see the section "Forelimb reach training"). All mice were randomly assigned to conditions and were precisely age-matched (±5 days) across experimental groups. *NG2–mEGFP* (The Jackson Laboratory, stock no. 022735) and congenic C57BL/6N *MOBP–EGFP* (MGI:4847238) lines, which have been previously described[19,23], were used for two-photon imaging. Wild-type C57\B6N Charles River wild-type mice were used in the electrophysiological experiments.

Two-photon microscopy. Cranial windows were prepared as previously described[19]. Six- to eight-week-old mice were anesthetized with isoflurane inhalation (induction, 5%; maintenance, 1.5–2.0%, mixed with 0.5 liter per min O_2) and kept at 37 °C body temperature with a thermostat-controlled heating plate. After removal of the skin over the right cerebral hemisphere, the skull was cleaned and a 2 × 2 mm region of skull centered over the forelimb region of the primary motor cortex (0–2 mm anterior to bregma and 0.5–2.5 mm lateral) was removed using a high-speed dental drill. A piece of cover glass (VWR, No. 1) was then placed in the craniotomy and sealed with Vetbond (3M) and then dental cement (C&B Metabond). A 5 mg per kg dose of carprofen was subcutaneously administered before awakening and for three additional days for analgesia. For head stabilization, a custom metal plate with a central hole was attached to the skull. In vivo imaging sessions began 2–3 weeks post-surgery and took place 2–3 times per week (see imaging timelines in Figs. 1–3 and 5). During imaging sessions, mice were anesthetized with isoflurane and immobilized by attaching the head plate to a custom stage. For *MOBP–EGFP* experiments, images were collected using a Zeiss LSM 7MP microscope equipped with a BiG GaAsP detector using a mode-locked Ti:sapphire laser (Coherent Ultra) tuned to 920 nm. *NG2–mEGFP* mice were imaged using a Bruker Ultima Investigator microscope equipped with Hamamatsu GaAsP detectors and a mode-locked Ti:sapphire laser (Coherent Ultra) tuned to 920 nm. The average power at the sample during imaging was 5–30 mW. Vascular and cellular landmarks were used to identify the same cortical area over longitudinal imaging sessions. *MOBP–EGFP* image stacks were acquired using a Zeiss W plan-apochromat ×20/1.0 NA water immersion objective giving a volume of 425 µm × 425 µm × 336 µm (1,024 × 1,024 pixels; corresponding to layers I–III, 0–336 µm from the meninges) from the cortical surface. *NG2–EGFP* image stacks were acquired using a Nikon LWD plan fluorite ×16/0.8 NA water objective with a volume of 805 µm × 805 µm × 336 µm (2,048 × 2,048 pixels; corresponding to layers I–III, 0–336 µm from the meninges).

SCoRe microscopy. SCoRe microscopy was performed as previously described[52]. For the *MOBP–EGFP* SCoRe/two-photon validation experiments, in vivo image stacks were acquired on an Olympus F1000MPE upright multiphoton microscope (DIVER). Single-photon confocal microscopy was performed using 488-, 543- and 633-nm laser lines combined with appropriate emission filters and descanned Olympus detectors. Two-photon microscopy of *MOBP–EGFP* fluorescence was performed immediately following SCoRe imaging using a mode-locked Insight X3 laser (Spectra-Physics) tuned to 920 nm and non-descanned Olympus detectors. All images were obtained using an Olympus ×20/1.0 NA water immersion objective (XLUMPLFLN20XW). SCoRe image channels were summed, registered to the two-photon data and then analyzed for SCoRe/two-photon colocalization using Fiji or ImageJ.

Cuprizone-mediated demyelination. Cortical demyelination was induced in our congenic C57\B6N *MOBP–EGFP* mice using 0.2% cuprizone (Sigma Chemical, C9012), stored in a glass desiccator at 4 °C. Cuprizone was mixed into powdered chow (Harlan) and provided to mice in custom feeders (designed to minimize exposure to moisture) for 3 weeks on an ad libitum basis. Feeders were refilled every 2–3 days, and fresh cuprizone chow was prepared weekly. Cages were changed weekly to avoid build-up of cuprizone chow in bedding, and to minimize reuptake of cuprizone chow following cessation of diet via coprophagia. We used a 3-week partial cortical demyelination model (resulting in 88.3 ± 2.9% oligodendrocyte loss in the motor cortex) to allow us to track the same area of interest over time using surviving oligodendrocytes, and to investigate the behavior of surviving oligodendrocytes. Given that cuprizone was ingested on a voluntary basis, we controlled for variations in dosage in several ways. First, we weighed a subset of mice ($n = 19$) before and after the cuprizone diet to ensure no weight loss had occurred. We found that on average, mice gained weight during cuprizone administration, confirming their consumption of the drug (paired Student's *t*-test, $t(18) = 2.32$, $P = 0.03$). Second, we investigated variations in total oligodendrocyte loss. There was variation in maximum oligodendrocyte loss (50–100%), and oligodendrocyte loss and gain had a partially homeostatic relationship in that the amount of loss significantly predicted the subsequent amount of oligodendrocyte gain (Fig. 3g; Extended Data Fig. 5). To control for variations in total oligodendrocyte loss, and its subsequent effects on oligodendrocyte gain, we therefore measured oligodendrocyte gain relative to the severity of loss using the following equation:

$$\text{Oligodendrocyte replacement}\ (\%) = \frac{\text{New oligodendrocytes}}{\text{Maximum oligodrendrocyte loss}} \times 100$$

Forelimb reach training. Mice were weighed, habituated to a training box for 20 min and deprived of food 24 h before training. The training box was fitted with a window providing access to a pellet located on a shelf 1-cm anterior and 1-mm lateral to the right-hand side of the window. After one session of initial habituation, training sessions began daily for 20 min. Mice learned to reach for the pellet using their left paw. Successes were counted when the mouse successfully took the pellet and transported it inside the box. Errors were qualified in the following three ways: 'reach error' (the mouse extends its paw out the window but does not grasp the pellet); 'grasp error' (the mouse reaches the pellet but does not successfully grasp onto it); and 'retrieval error' (the mouse grasps the pellet but does not succeed in returning it to the box) (Supplementary Video 1). Mice were kept on a restricted diet throughout training to maintain food motivation, but were weighed daily to ensure weight loss did not exceed 10%. For forelimb reach training, mice underwent habituation (average of ~2 days of exposure) followed by training until seven consecutive days of training with reach attempts were recorded. For the rehearsal of the forelimb reach task, mice performed the reach task in a 20-min session, 5 days per week over 3 weeks. Similar to previously published findings[18], over 90% of mice trained in the forelimb reach context were able to learn the task; mice were excluded if on a single day they were not able to succeed in at least 10% of reaches (Extended Data Fig. 1). To control for any batch or experimenter effects on the forelimb reach training results, behavioral performance was only compared for mice trained by the same experimenter within the same batch (that is, control and experimental mice were only compared if trained at the same time by the same experimenter).

Immunohistochemistry. Mice were anesthetized with an intraperitoneal injection of sodium pentobarbital (100 mg per kg body weight) and transcardially perfused with 4% paraformaldehyde in 0.1 M phosphate buffer (pH 7.0–7.4). Brains were postfixed in 4% paraformaldehyde for 1 h at 4 °C, transferred to 30% sucrose solution in PBS (pH 7.4) and stored at 4 °C for at least 24 h. Brains were extracted, frozen in TissuePlus OCT and sectioned coronally or axially (bregma 0–2 mm) at 50-µm thick. Immunostaining was performed on free-floating sections. Sections were preincubated in blocking solution (5% normal donkey serum, 2% bovine γ-globulin, 0.3% Triton X-100 in PBS, pH 7.4) for 1–4 h at room temperature, then incubated overnight at 4 °C in primary antibody (listed along with secondary antibodies in Supplementary Table 1). Secondary antibody incubation was performed at room temperature for 2 h. Sections were mounted on slides with Vectashield antifade reagent (Vector Laboratories). Images were acquired using a laser-scanning confocal microscope (Zeiss LSM 510).

Image processing and analysis. Image stacks and time series were analyzed using Fiji or ImageJ. All analyses were performed on unprocessed images except for analyses of surviving oligodendrocyte myelin sheath images, which were preprocessed using a Gaussian blur filter (radius = 1 pixels) to denoise. When generating figures, image brightness and contrast levels were adjusted for clarity. For the pseudocolor display of individual myelin sheaths or OPCs (Figs. 1–4, 6 and 7; Extended Data Figs. 2, 4, 8–10; Supplementary Videos 2, 3, 5, 6, 8–17), a maximum projection of the region of interest was generated and was manually segmented and colorized. Longitudinal image stacks were registered using the Fiji plugins Correct 3D drift[53] or PoorMan3DReg. When possible, blinding to experimental conditions was used for analyzing image stacks from two-photon imaging. To ensure the validity of oligodendrocyte lineage cell tracking, we performed interrater reliability on a subset of images and found a highly significant correlation between raters ($R^2 = 0.998$, $P < 0.0001$).

Cell tracking. Custom Fiji scripts were written to follow oligodendrocytes in four dimensions by defining $EGFP^+$ cell bodies at each time point, recording *x*, *y* and *z* coordinates, and defining cellular behavior (new, dying, proliferating, differentiating or stable cells). Mature oligodendrocyte and OPC migration, proliferation, death and differentiation were defined as previously described[19,23]. Differentiation events were recorded as the time point immediately preceding the total loss of NG2–mEGFP fluorescence. OPC and oligodendrocyte gain and loss were cumulatively quantified relative to the baseline cell number to account for variations in the starting cell number. The rate of oligodendrocyte gain was quantified as the percentage change in gain over the amount of time elapsed.

Identification of surviving oligodendrocytes. A subset of surviving oligodendrocytes exhibited drastic changes in morphology during remyelination in the form of cell body expansion, sheath addition and increase in EGFP expression (Extended Data Figs. 8–10). To ensure that these oligodendrocytes were in fact individual surviving oligodendrocytes and not new oligodendrocytes generated in a similar location

that myelinated similar axonal locations, we employed the following criteria for inclusion in our final dataset:

1. Change in cell soma centroid (<2.5 standard deviations from the mean)
2. Percentage of sheath retention (>10% of original sheaths)
3. Change cell soma volume (<700 μm^3)
4. Protracted sheath addition (>6 days)
5. Semiautomated tracing of new sheath to oligodendrocyte surviving cell body (using Simple Neurite Tracer)
6. Distance between surviving and new oligodendrocyte cell bodies at time point of sheath generation (>50 µm)

Due to the stringency and conservative nature of these criteria, we consider our findings to likely be an underestimate of the capacity of surviving oligodendrocytes to generate new myelin sheaths. We measured the change in centroid position of surviving oligodendrocyte cell bodies from baseline to the day of peak remodeling—that is, the day at which the largest number of sheaths were added by a given oligodendrocyte. We ensured that the three-dimensional location of individual surviving oligodendrocytes did not change by more than 2.5 standard deviations from the mean displacement of reference objects measured within the same stack (5.459 ± 2.373 µm; Extended Data Fig. 8). Since myelin sheath loss occurs significantly earlier than cell body loss in oligodendrocyte cell death (Fig. 3d,e), and a new oligodendrocyte could be generated in the same location immediately following the death of the original oligodendrocyte, we only included surviving oligodendrocytes that conserved at least 10% of their original processes (mean percentage of conserved processes = 75.6 ± 4.45%). There is an increase in the frequency of pairs and rows of oligodendrocytes with adjacent cell somas in the aging brain[54]. Since the axial resolution of our two-photon microscope is ~2.6 µm, we should be able to resolve two directly adjacent oligodendrocytes in the *z* direction. To ensure that this is the case, we took several additional steps to rule out the addition of a new oligodendrocyte generated immediately adjacent in the *z* axis. Reduction of cell soma size is a hallmark of the maturation of OPCs into myelinating oligodendrocytes[50,51]; therefore, we measured the cell soma volume of newly generated oligodendrocytes (Extended Data Fig. 8). Next, we measured each surviving oligodendrocyte at baseline and at the day of peak remodeling to determine the change in cell soma volume. Assuming a *z* distance of 0 µm between two cells, we excluded oligodendrocytes that grew more than 700 μm^3, which is the volume of the smallest new oligodendrocyte measured (Extended Data Fig. 8). Additionally, we ensured that this growth was not unidirectional (as you would see with the addition of an adjacent oligodendrocyte cell body), but rather that the oligodendrocyte cell body expanded in multiple directions around the centroid position. Previous studies have indicated that new oligodendrocytes have a limited period in which to generate all of their myelin sheaths; for example, a few hours in the developing zebrafish[55] and less than 18 h in vitro[56]. We found that new oligodendrocytes generate all sheaths within 0–3 days of generation in mice ($n_{mice} = 11$; $n_{cells} = 26$; Fig. 4). If a new oligodendrocyte was generated directly adjacent to a surviving oligodendrocyte, we would predict that all additional myelin sheaths would be added within this time frame. Therefore, we required that surviving oligodendrocytes that added more than four sheaths—approximately 10% of the average sheaths generated by an oligodendrocyte—must have added these new sheaths over multiple, nonconsecutive imaging time points (Extended Data Fig. 8; Supplementary Video 14). Using these criteria, two oligodendrocytes were excluded from the final dataset as they may have represented the addition of a new oligodendrocyte in a similar location. One oligodendrocyte violated both the change in centroid requirement and protracted sheath addition requirement (change in centroid = 19.3266 µm, and 8 sheaths were added at one time point), and the other violated the terms for protracted sheath addition (over ten sheaths added within two consecutive time points). Three other surviving oligodendrocytes were excluded from the new sheath analysis because new oligodendrocytes were generated within 50 µm of the surviving oligodendrocyte cell body on the day of surviving oligodendrocyte sheath addition. The surviving oligodendrocyte dataset was analyzed by multiple, blinded raters and, where blinding was not possible (for example, due to recognizable landmarks in the image stacks), all counts were validated by multiple raters. As an additional measure, only new sheaths with processes that could be traced back to the surviving oligodendrocyte cell body with Simple Neurite Tracer were included in our final dataset (Extended Data Fig. 2; Supplementary Video 3). Finally, myelin debris prevented a faithful analysis of processes and sheaths from oligodendrocytes in the time point following cuprizone treatment; therefore, we excluded the time point immediately after the removal of cuprizone (that is, 0 day) from analysis.

Myelin sheath analysis of individual oligodendrocytes. In vivo *z* stacks were collected from *MOBP–EGFP* mice using two-photon microscopy. The *z* stacks were processed with a 1-pixel Gaussian blur filter to aid in the identification of myelin internodes. Myelin paranodes and nodes of Ranvier were identified as previously described[19] by increasing the fluorescence intensity for paranodes and decreasing to zero the EGFP fluorescence intensity for nodes. Myelin sheaths from surviving oligodendrocytes were traced using Simple Neurite Tracer at day −25 and day 21. In normal learning mice, two additional time points were traced that corresponded to day 0 and day 9 of training. To account for differences in measurement due to tracing, a subset of sheaths were traced five times at a single time point. Traces of the same sheath differed by less than 5.56 µm. Therefore, sheaths were defined as stable if their baseline and final lengths changed by less than 5.56 µm. Sheaths that grew more than 5.56 µm were considered growing and those that shrank more than 5.56 µm were considered retracting.

For myelin sheath analysis of surviving oligodendrocytes, surviving oligodendrocytes that resided within a volume of 425 × 425 × 100 μm^3 from the pial surface were considered in layer I and cells 100–336 μm^2 were considered layer II/III. Myelin sheaths of surviving oligodendrocytes were tracked throughout time with the same Fiji scripts used for cell tracking. Only sheaths with visible processes back to the surviving cell body in at least one time point were counted. Sheaths were defined as new, lost or persisting. Persisting sheaths lasted for the entire imaging time course, new sheaths appeared after day 0, and lost sheaths disappeared before the end of the imaging time course and were not visible for at least two consecutive time points. Our average total sheath count per surviving oligodendrocyte was 30.2 ± 1.32. Assuming a normal range of 45 ± 4 sheaths per oligodendrocyte[19], our average sampling was 67–74% of all sheaths.

Electrophysiology. Chronic in vivo recordings were conducted during 20-min forelimb reach training sessions before, during and after cuprizone treatment. A single 1.6-mm vertical NeuroNexus recording electrode was chronically inserted into the primary motor cortex (300 µm anterior to bregma, 1.5 mm lateral to bregma) contralateral to the trained forelimb. Data were recorded using Cheetah acquisition software at 30 kHz (NeuroNexus), and single-unit activity was clustered using Spike Sort 3D (Neuralynx). Isolation distance and L-ratio were used to quantify cluster quality and noise contamination[57]. Spike data were binned at 10 ms and trial-averaged. Heatmaps report the average firing rate during a 500-ms time window when the animal was not engaged in reaching behavior.

Statistics. A detailed and complete report of all statistics used, including definitions of individual measures, summary values, sample sizes and all test results, can be found in Supplementary Table 2. Sample sizes were not predetermined using statistical methods, but were comparable to relevant publications[19,23]. All data were initially screened for outliers using interquartile range (IQR) methods. In Fig. 7j, a single outlier oligodendrocyte was removed after testing because it drove significance in the correlation (see Supplementary Table 2 for details). Homozygous, C57BL/6N congenic *MOBP–EGFP* mice were bred with C57BL/6N mice to generate litters of experimental mice that were hemizygous for the *MOBP–EGFP* transgene. All mice in a litter underwent cranial window surgery, concurrent two-photon imaging timelines and were designated to be a batch. When possible, experimental groups were replicated in multiple batches with multiple experimental groups per batch. However, due to the longitudinal nature of our study and the clarity of cranial windows used to conduct two-photon imaging, we could not predict which mice would produce full datasets when assigning them to the experimental conditions. As a result, not all batches contain all experimental groups, and we statistically controlled for batch effects. Statistical analyses were conducted using JMP (SAS) or Matlab (MathWorks). We first assessed normality in all datasets using the Shapiro–Wilk test. When normality was violated, we used nonparametric tests. When normality was satisfied, we used parametric statistics, including paired or unpaired two-tailed Student's *t*-tests (depending on the within- or between-subjects nature of the analysis), or analysis of variance (ANOVA) with Tukey's honestly significant difference (HSD) post-hoc tests. Two-tailed tests and $\alpha \leq 0.05$ were always employed unless otherwise specified. For statistical mixed modeling, we used a restricted maximum likelihood approach with an unbounded variance component and least-squared Tukey's HSD post-hoc tests. All models were conducted with either one or two fixed effects, in which case we ran full factorial models. For all models, we used 'Mouse ID' as a random variable, and this random variable was nested within batch if data came from separate batches. Where we found significant effects, we subsequently calculated the effect size using test-appropriate approaches. For data visualization, all error bars represent the standard error of the mean, all bar graphs denote means and all box plots illustrate medians and IQRs unless otherwise specified. We used 3P logistic equation modeling to fit sigmoidal curves bound between an asymptote of 0 (baseline) and an estimated plateau to oligodendrocyte accumulation (either loss or gain) across time.

Reporting Summary. Further information on research design is available in the Nature Research Reporting Summary linked to this article.

Data availability

All data that support the findings, and the tools and reagents will be shared on an unrestricted basis; requests should be directed to the corresponding author.

Code availability

All published code will be shared on an unrestricted basis; requests should be directed to the corresponding authors.

References

52. Schain, A. J., Hill, R. A. & Grutzendler, J. Label-free in vivo imaging of myelinated axons in health and disease with spectral confocal reflectance microscopy. *Nat. Med.* **20**, 443–449 (2014).
53. Parslow, A., Cardona, A. & Bryson-Richardson, R. J. Sample drift correction following 4D confocal time-lapse imaging. *J. Vis. Exp.* **86**, e51086 (2014).
54. Peters, A. & Sethares, C. Oligodendrocytes, their progenitors and other neuroglial cells in the aging primate cerebral cortex. *Cereb. Cortex* **14**, 995–1007 (2004).
55. Czopka, T., ffrench-Constant, C. & Lyons, D. A. Individual oligodendrocytes have only a few hours in which to generate new myelin sheaths in vivo. *Dev. Cell* **25**, 599–609 (2013).
56. Watkins, T. A., Emery, B., Mulinyawe, S. & Barres, B. A. Distinct stages of myelination regulated by γ-secretase and astrocytes in a rapidly myelinating CNS coculture system. *Neuron* **60**, 555–569 (2008).
57. Schmitzer-Torbert, N., Jackson, J., Henze, D., Harris, K. & Redish, A. D. Quantitative measures of cluster quality for use in extracellular recordings. *Neuroscience* **131**, 1–11 (2005).

Acknowledgements

We thank A. Chavez for technical assistance; A. Scallon and the Optogenetics and Neural Engineering Core (P30NS048154); D. Stitch and the University of Colorado Anschutz Medical Campus Advance Light Microscopy Core (P30NS048154); M. Hall for machining expertise; S. Bromley-Coolidge for assistance with reach videos; S. Rock Levinson for discussions on 3P logistic equation modeling; B. Cudmore (UC Davis College of Biological Sciences) for image processing expertise; M. Rasband (Baylor College of Medicine) for providing the βIV spectrin (C9581) antibody; M. Bhat (UT Health San Antonio) for providing the Caspr antibody; and members of the Hughes and Welle labs for discussions. M.A.T. is supported by the NIH Institutional Neuroscience Graduate Training Grant (5T32NS099042-17). Funding was provided by NIH 1R21EY029458-01 and the Boettcher Foundation Webb–Waring Biomedical Research Award to C.G.W. and the Boettcher Foundation Webb–Waring Biomedical Research Award, the Whitehall Foundation, the Conrad N. Hilton Foundation (17324), and the National Multiple Sclerosis Society (RG-1701–26733) and NINDS (NS106432, NS115975) to E.G.H.

Author contributions

E.G.H. and C.R.M. conceived the project. C.M.B. designed, analyzed and generated Figs. 1, 4, 6 and 7, Extended Data Figs. 2, 4, 8–10 and Supplementary Videos 2–17. H.J.B. designed, analyzed and generated Figs. 1, 3, 5 and 6, Extended Data Figs. 1, 3, 5–7, Supplementary Fig. 1 and Supplementary Video 1. C.R.M. contributed to the data analysis in Figs. 1, 3 and 5 and Extended Data Figs. 1 and 4–6. M.A.T. designed, analyzed and generated Fig. 2 and Extended Data Figs. 2–4. D.N. performed all electrophysiological experiments and analyses. C.G.W. supervised the electrophysiological experiments. E.G.H. supervised the project. C.M.B., H.J.B. and EGH wrote the manuscript with input from other authors.

Competing interests

The authors declare no competing interests.

Additional information

Extended data is available for this paper at https://doi.org/10.1038/s41593-020-0637-3.

Supplementary information is available for this paper at https://doi.org/10.1038/s41593-020-0637-3.

Correspondence and requests for materials should be addressed to E.G.H.

Reprints and permissions information is available at www.nature.com/reprints.

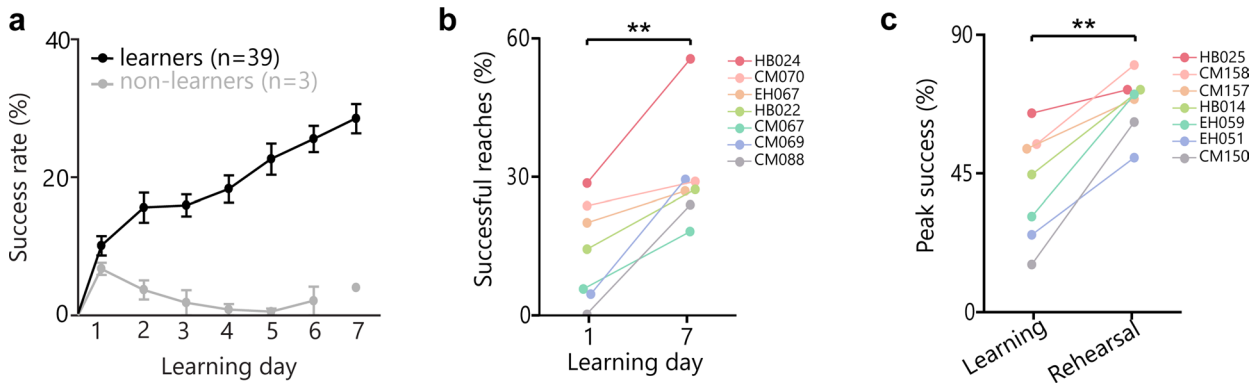

Extended Data Fig. 1 | Learning and rehearsal of a forelimb reach task induce skill refinement. a, A large majority (93%) of mice successfully learn to perform the forelimb reach task. 'Learners' (black) gradually improve their reaching performance over the seven days of training, whereas 'non-learners' (grey) show a progressive decrease in success rate and eventually stop making reach attempts around day 4. Note, the lone point in the 'non-learner' group at day 7 is due to only one mouse making attempts on the last day of training. The other two mice had stopped trying. **b**, Successful reaches (%) significantly increase between learning days 1 and 7 (paired samples t-test; $t(6) = 4.80$, $p = 0.003$) for mice placed in 'learning' group. c, Peak performance during rehearsal (successful reaches; %) is significantly higher than peak performance during learning (paired samples t-test; $t(6) = 5.47$, $p = 0.0016$) for mice placed in 'rehearsal' group. Individual colors and traces reflect performance by individual mice. *$p < 0.05$, **$p < 0.01$, ***$p < 0.001$. *Bars and errors represent Mean ± SEM, for statistics see* Supplementary Table 2.1.

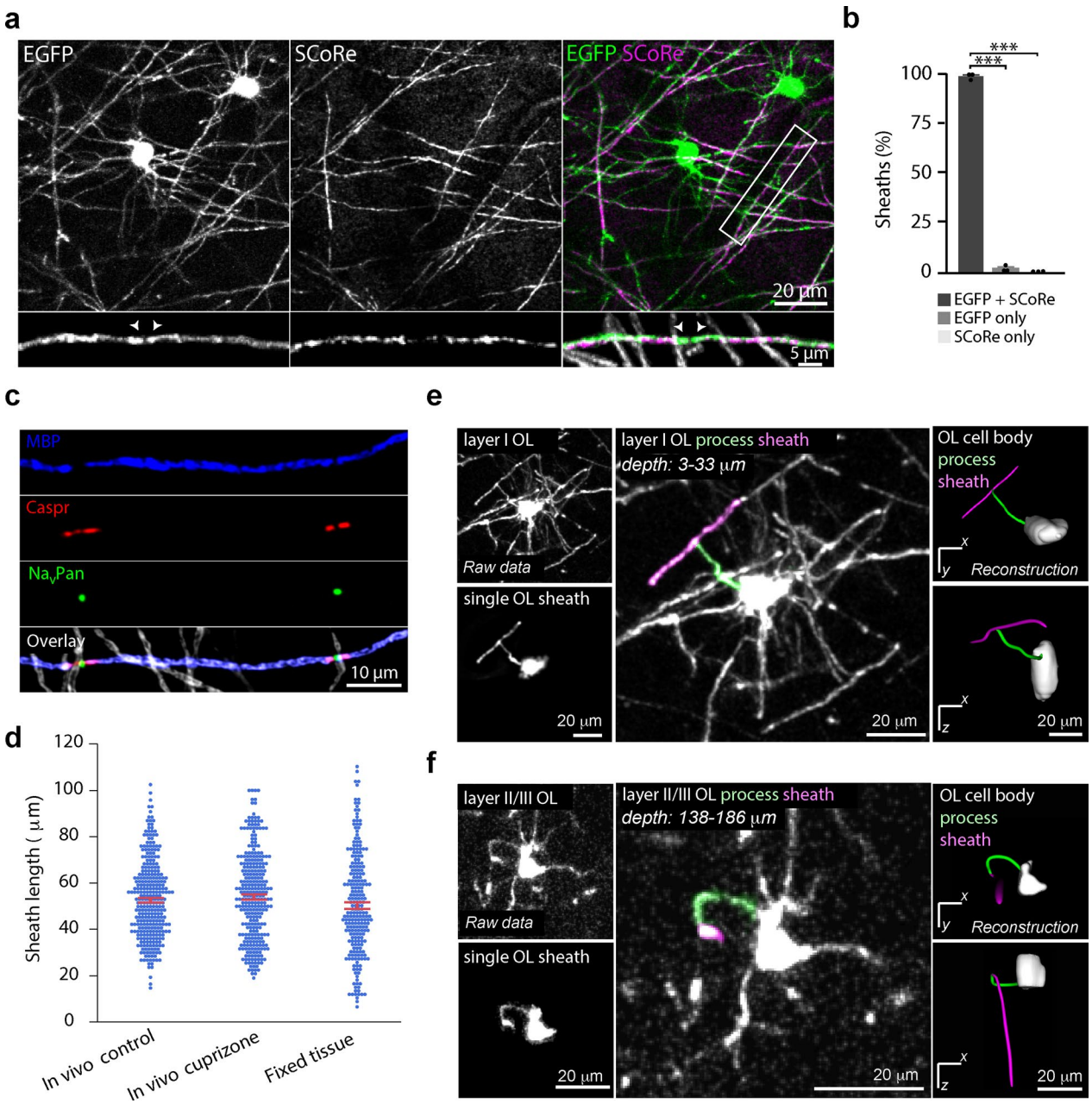

Extended Data Fig. 2 | *In vivo* imaging of *MOBP-EGFP* faithfully reflects myelin sheath presence, length, and connection to oligodendrocyte cell body. a, b, Maximum projections of cortical oligodendrocytes showing 98.24 ± 0.92% colocalization of *in vivo MOBP-EGFP* and SCoRe signal in myelin sheaths, confirming *MOBP-EGFP* faithfully reflects presence of myelin (ANOVA, $n_{mice} = 3$, $F_{2,6} = 5596.220$, $p < 0.0001$). **c**, Maximum projection of 4% paraformaldehyde fixed tissue, stained for myelin (blue, MBP), paranodes (Caspr, red), and sodium channels (NavPan, green). **d**, No significant difference between sheath lengths measured using Simple Neurite Tracer in *in vivo* two-photon images of control and cuprizone-treated *MOBP-EGFP* mice, and in confocal images of sheaths immunostained for MBP in fixed tissue ($n_{sheaths}$ = 306, 297 and 233, respectively; points represent individual sheaths; ANOVA; $F_{2,833} = 2.53$, $p > 0.08$; red points and error bars represent group means ± SEM). **e,f** Semi-automated tracing with Simple Neurite Tracer faithfully reconstructs oligodendrocyte myelin sheaths and their connecting processes to the cell soma in layer I (e) and layer II/II (f). Top left: Maximum projection of an oligodendrocyte (OL) imaged using *in vivo* two-photon microscopy, spanning a depth of 3–33 µm (e) and 138–186 µm (f) in motor cortex. Bottom left: maximum projection of an isolated single sheath and process attached to the oligodendrocyte cell body. Center: maximum projection and pseudo-colored sheath and process (sheath and process pseudo-colored). Right: Three-dimensional (3D) reconstruction of the same oligodendrocyte generated from the raw *in vivo* imaging data using the Simple Neurite Tracer plugin in FIJI. View of 3D volume in xy plane from below (top) and view of 3D volume through z (bottom). *$p < 0.05$, **$p < 0.01$, ***$p < 0.001$. *Bars and errors represent Mean ± SEM, for statistics see* Supplementary Table 2.1.

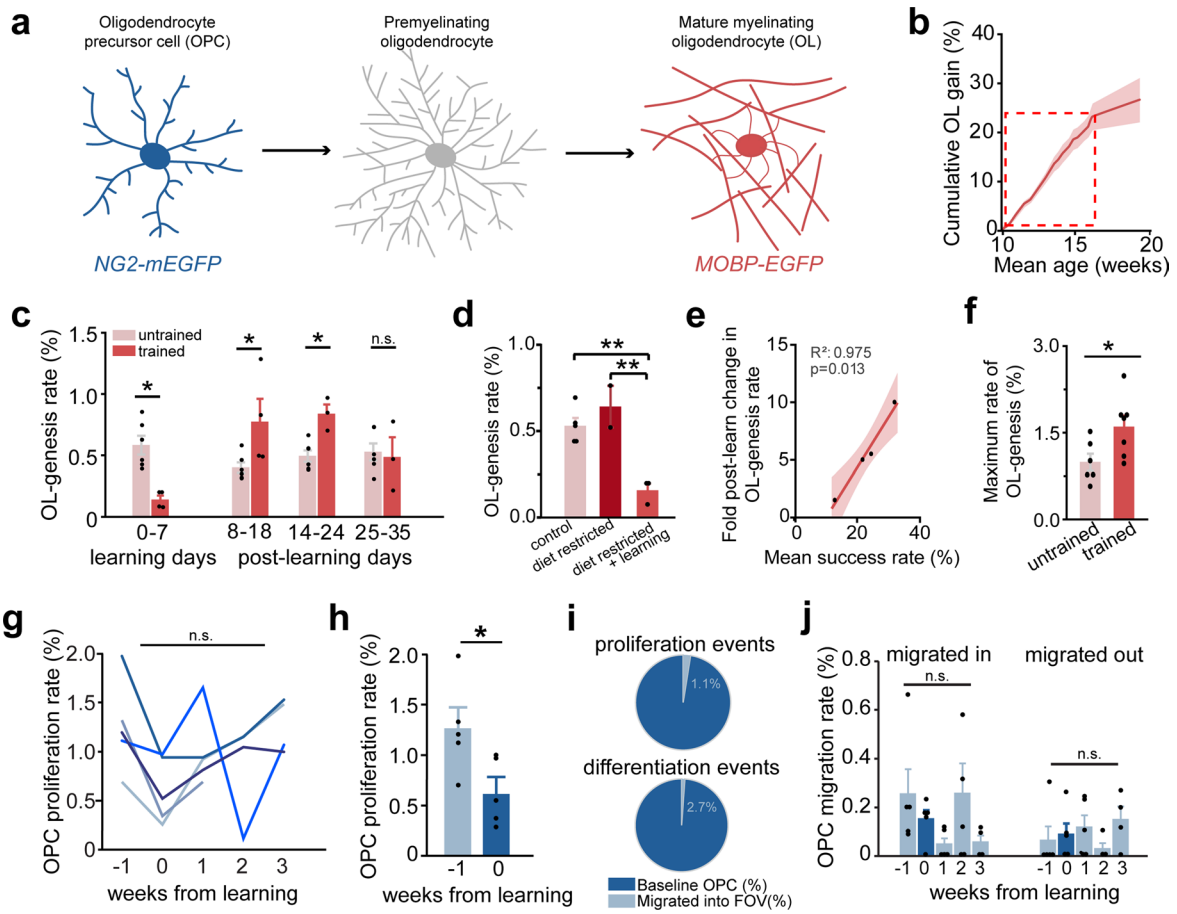

Extended Data Fig. 3 | Oligodendrocyte lineage cell dynamics throughout motor learning. a, Genetic lines for *in vivo* imaging of oligodendrocyte precursor cells (OPCs; *NG2-mEGFP*) and oligodendrocytes (OLs; *MOBP-EGFP*). **b**, Motor cortex oligodendrogenesis from age 10–20 weeks across six mice, showing a plateau ~17 weeks. Dashed box represents age during standard experimental timeline. **c**, Rate of oligodendrogenesis is altered in learning vs. untrained mice during learning (Wilcoxon Rank-Sum, $p = 0.014$), days 8–18 post-learning ($p = 0.038$), and days 14–24 post-learning ($p = 0.024$). No differences are observed by days 25–35 post-learning ($p > 0.9$). Points represent mice. **d**, Main effect of diet restriction on oligodendrogenesis rate (%; ANOVA; $F_{2,8} = 18.13$, $p = 0.001$). Diet-restricted and non-diet-restricted controls have higher rates of oligodendrogenesis than diet-restricted learning mice (Tukey's HSD, $p = 0.001$ and $p = 0.005$, respectively). **e**, Mean success rate is related to fold change in oligodendrogenesis rate post-learning (R-square = 0.98, $p = 0.01$). Line and shaded area represent fit and 95% confidence of fit. **f**, Trained mice (learning and rehearsal) have increased maximum rates of oligodendrogenesis relative to controls ($t(10.61) = -2.49$, $p = 0.03$). **g, h**, Proliferation rates from Fig. 2d; colors represent individual mice. All mice show reduced proliferation rate during learning relative to baseline ($t(4) = -3.89$, $p = 0.018$; paired student's t-test), but no main effect of time on proliferation rate across the five weeks of experiment - possibly due to high variability post-learning ($F_{4,15} = 2.341$). **i**, Only a minority of proliferation and differentiation events occurred in OPCs that had migrated into the field of view throughout the course of the experiment. **j**, No effect of learning on rate of migration into or out of the field of view. *$p < 0.05$, **$p < 0.01$, ***$p < 0.001$. *Bars and errors represent Mean ± SEM, for statistics see* Supplementary Table 2.1.

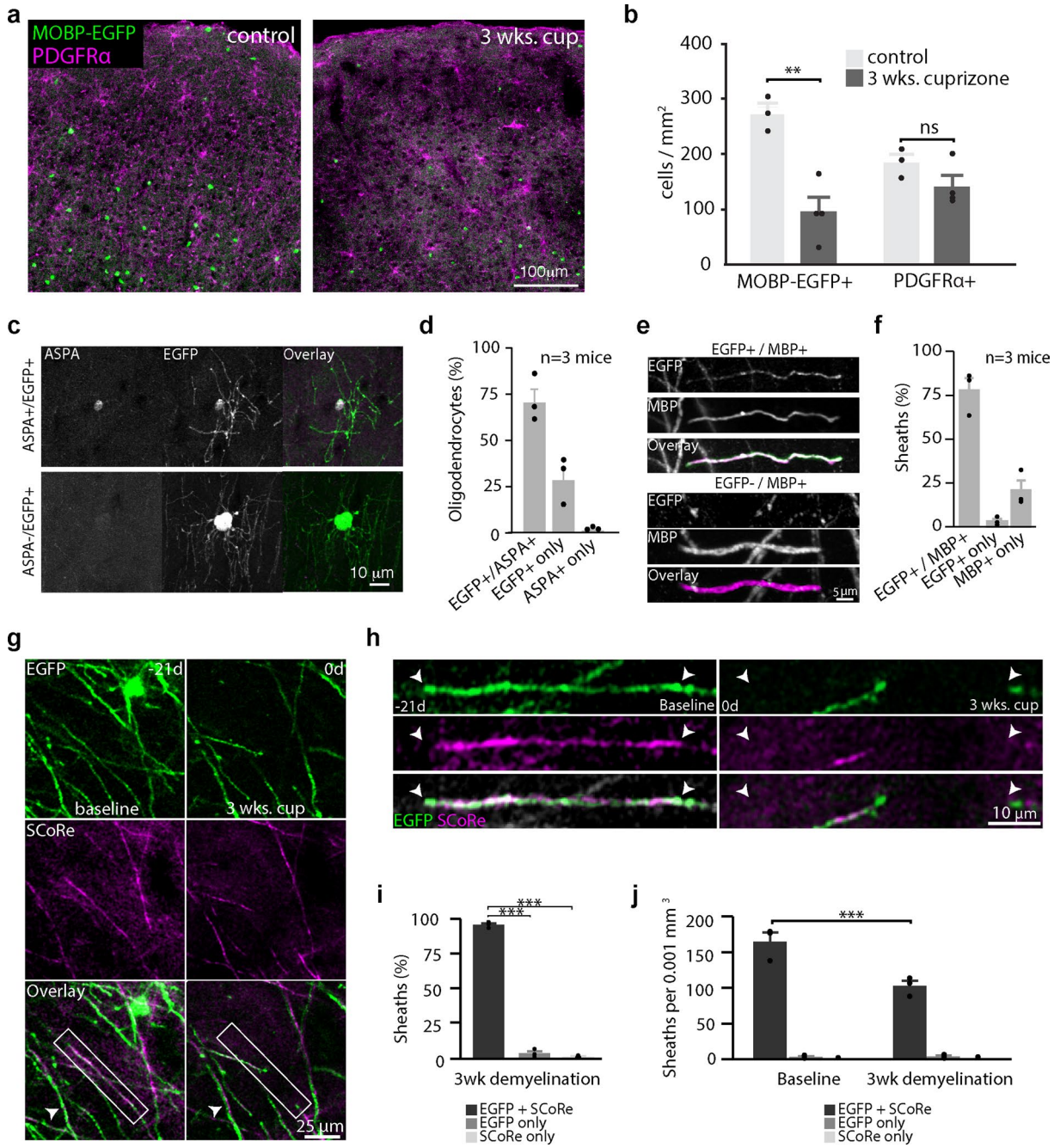

Extended Data Fig. 4 | Cuprizone treatment results in loss of myelin and oligodendrocytes. a, b, Mean density of EGFP+ and PDGFRα+ cells in control and cuprizone-treated *MOBP-EGFP* mice; individual points represent individual mice. Interaction effect between drug (control vs. cuprizone) and cell type (EGFP+ vs PDGFRα+; ($F_{1,5}=22.39$, $p=0.0052$) to predict cell density. While EGFP+ cell density is decreased in cuprizone-treated mice relative to controls (Tukey's HSD; $p=0.0086$), there is no difference in PDGFRα+ cells between groups ($p>0.5$). **c**, Maximum projection of a EGFP⁺/ASPA⁺ oligodendrocyte (top) and a EGFP⁺/ASPA⁻ oligodendrocyte (bottom). Note the large size of the ASPA⁻/EGFP⁺ cell soma suggesting it is a recently born oligodendrocyte in the early stages of the maturation process. **d**, After three weeks of cuprizone treatment, 70.73±12.78% of oligodendrocytes are EGFP⁺/ASPA⁺, 0.97±0.84% of cells are ASPA⁺/EGFP⁻, while the remainder are EGFP± only ($n_{mice}=3$, $n_{cells}=185$). **e**, Maximum projection of an MBP⁺ myelin sheath with (top) and without EGFP (bottom) after three weeks of cuprizone. **f**, After three weeks of cuprizone, 76.21±7.11% of sheaths are MBP⁺/EGFP⁺, and 20.6±5.79% of sheaths are MBP⁺/EGFP⁻ ($n_{mice}=3$, $n_{sheaths}=351$). **g, h** Maximum projections of oligodendrocytes showing colocalization of *in vivo MOBP-EGFP* and SCoRe imaging for myelin both before cuprizone administration (−21 days) and immediately following its removal (0 days). Note the surviving sheath (white arrow). **i**, Following 3 weeks of cuprizone diet, most myelin sheaths are MOBP-EGFP⁺/SCoRe⁺ (95.71±1.16; ANOVA, $F_{2,6}=2012.94$, $p<0.0001$). **j**, Cuprizone administration modulates sheath density ($F_{2,10}=14.43$, $p=0.001$). Cuprizone-fed mice have a reduced density of MOBP-EGFP⁺/SCoRe⁺ positive sheaths relative to controls ($p=0.0001$), but no difference in GFP-only or SCoRe-only sheaths. *$p<0.05$, **$p<0.01$, ***$p<0.001$. *Bars and errors represent Mean±SEM, for statistics see* Supplementary Table 2.3.

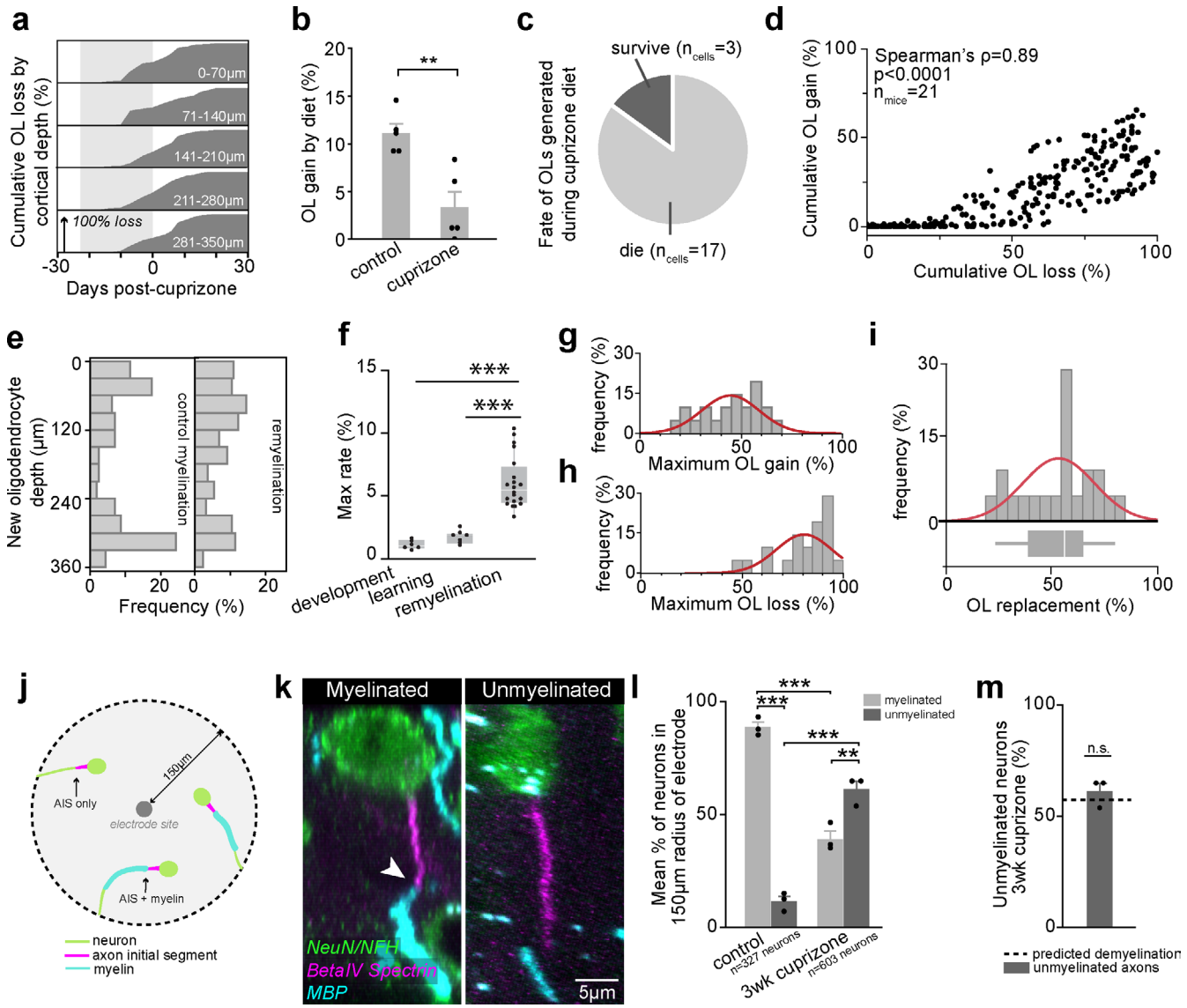

Extended Data Fig. 5 | Dynamics of oligodendrocyte generation and loss during cuprizone treatment. a, Oligodendrocyte loss occurred evenly across cortical depths. Shaded area represents cuprizone diet. **b**, Oligodendrogenesis is suppressed during cuprizone diet (n = 5 mice per group; $t(6.54) = 4.10$, $p = 0.005$; Student's t-test). **c**, 85% of oligodendrocytes generated during cuprizone diet die within three weeks. **d**, Oligodendrocyte loss predicts gain (Spearman's $\rho = 0.89$). **e**, Oligodendrocytes generated during remyelination are distributed across cortex similarly to developmental oligodendrogenesis (Wilcoxon Rank-sum, $p > 0.1$). **f**, Remyelination alters oligodendrogenesis rates ($F_{29,2} = 27.67$, $p < 0.0001$; ANOVA). Rates are higher during remyelination than in healthy trained and untrained mice ($p < 0.0001$ and $p < 0.0001$, respectively; Tukey's HSD). **g–i**, Inter-individual variation in oligodendrocyte gain and loss is controlled for by normalizing gain to loss ('oligodendrocyte replacement'). **j, k**, Representative diagram and images of peri-electrode immunohistochemistry. Myelinated neurons within 150 microns of the electrode (indicated with white arrowhead; layer II/III XZ maximum projection) were co-labelled with MBP (myelin; cyan), beta-IV spectrin (axon initial segment; purple) and NeuN/NFH (neuron cell soma / distal axon; green; top), whereas unmyelinated axons did not co-localize with MBP (bottom). **l**, Cuprizone administration alters peri-probe axonal myelination (Two-way ANOVA; $F_{3,8} = 110.51$, $p < 0.0001$). Control mice have more myelinated versus unmyelinated axons (Tukey's HSD, $p < 0.0001$). At the cessation of cuprizone, cuprizone-fed mice have fewer myelinated ($p < 0.0001$) and more unmyelinated axons than healthy controls ($p < 0.0001$), and more unmyelinated than myelinated axons ($p = 0.004$). *Note: myelin may be present elsewhere on the axon.* **m**, The proportion of unmyelinated neurons observed via IHC does not differ from the proportion of myelin loss predicted by sigmoidal demyelination characterized in Fig. 3e-h (one-sample t-test, $t(2) = 1.10$, $p > 0.3$). *$p < 0.05$, **$p < 0.01$, ***$p < 0.001$. Bars and errors represent Mean ± SEM, points represent individual mice, for statistics see* Supplementary Table 2.3.

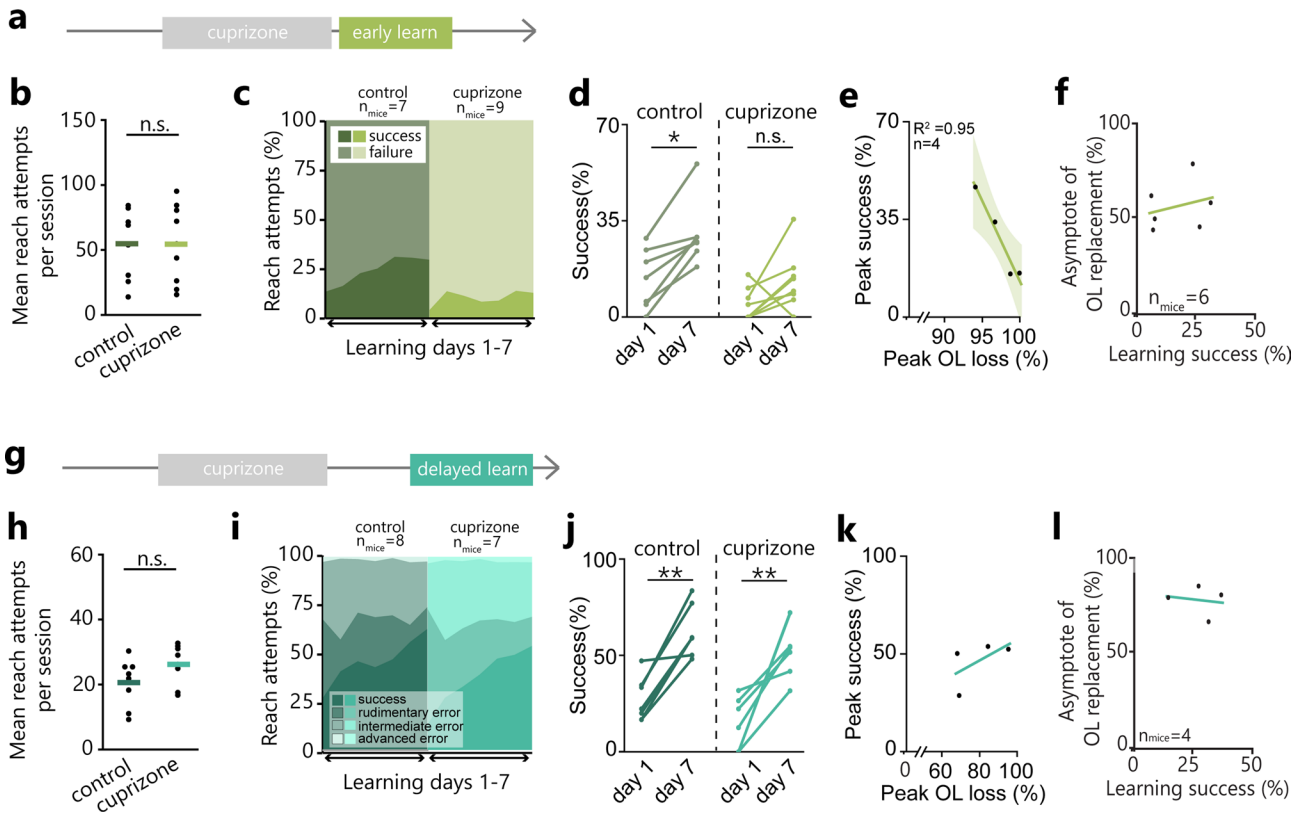

Extended Data Fig. 6 | Demyelination induces deficits in early, but not delayed, motor learning. a, Timeline for 'early-learning' intervention (3 days post-cuprizone). **b**, No difference in mean reach attempts per session during early-learning between control and cuprizone-treated mice (Student's t-test, $t(12.95) = 0.05$, $p > 0.9$; coloured lines represent group means). **c**, Area plot of reach attempt outcome (success vs. failure) across forelimb reach learning days in both control and cuprizone-treated mice. **d**, Control mice have improved success rates day 7 of training relative to day 1 (Paired Student's T-test; $t(6) = 4.7$, $p = 0.003$), but cuprizone-treated mice do not ($t(7) = 1.96$, $p = 0.09$). **e**, Maximum oligodendrocyte loss is related to peak performance during training ($R^2 = 0.95$, $p = 0.02$; line and shaded area represent line of fit and 95% confidence). **f**, No relationship between mean learning success rate (%) and asymptote of oligodendrocyte replacement in early learners. **g**, Timeline for 'delayed-learning' intervention (10 days post-cuprizone) **h**, No difference in mean reach attempts per session during delayed-learning between control and cuprizone-treated mice (Student's t-test, $t(12.95) = 1.54$, $p > 0.1$; coloured lines represent group means). **i**, Area plot of reach attempt outcome (success, rudimentary error, intermediate error, advanced error; see Supplementary Video 1) across delayed-learning days in both control and cuprizone-treated mice. **j**, Both control and cuprizone-treated mice improve their reaching success between days 1 and 7 of delayed-learning (Paired student's t-test, $p = 0.0005$ and $p = 0.004$, respectively). **k**, No relationship between maximum oligodendrocyte loss and reaching performance during delayed learning. **l**, No relationship between delayed learning success rate and asymptote of oligodendrocyte replacement post-cuprizone. *$p < 0.05$, **$p < 0.01$, ***$p < 0.001$. *Points represent individual mice, for statistics see* Supplementary Table 2.5.

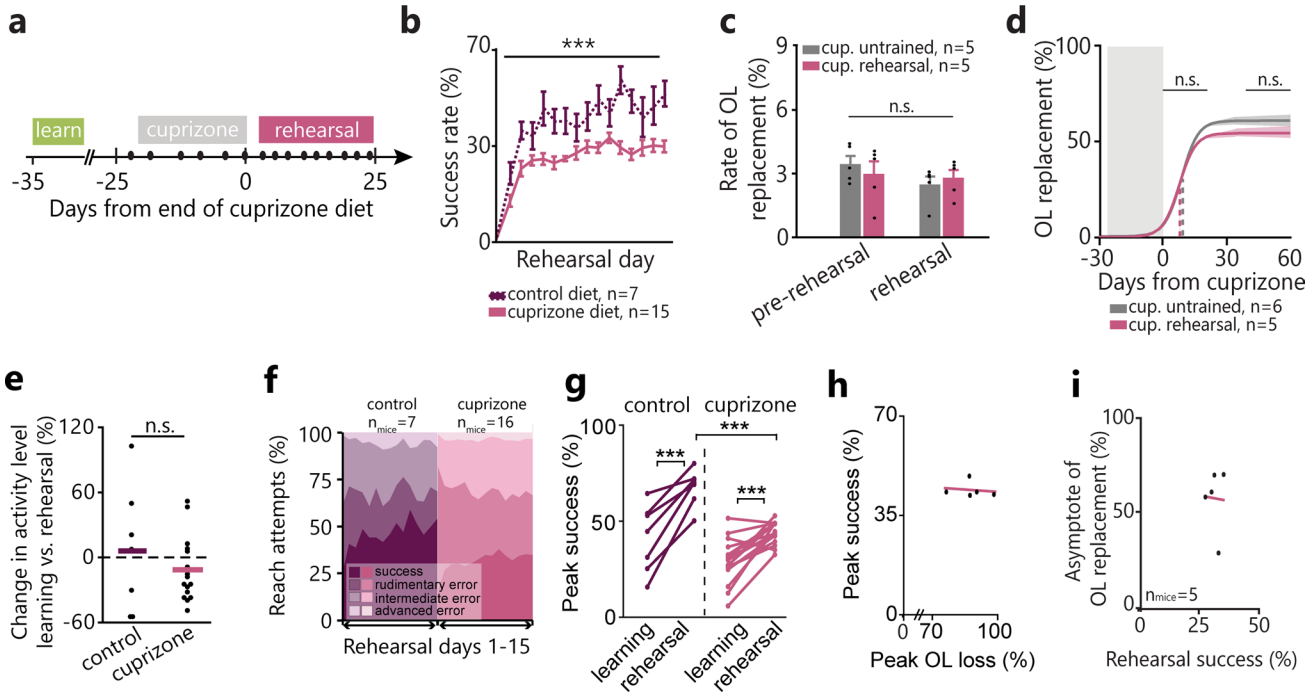

Extended Data Fig. 7 | Motor skill rehearsal does not modulate remyelination. a, Timeline of reach task rehearsal post cuprizone diet. **b**, Main effect of drug on reaching success during rehearsal ($F(1,14) = 27.73$, $p < 0.0001$). **c,d**, No effect of rehearsal on rate, inflection point, or asymptote of oligodendrocyte replacement. **e**, No effect of cuprizone on change in reaching behavior between learning and rehearsal. **f**, Area plot of reach attempt outcomes in control and cuprizone-demyelinated mice. **g**, Interaction effect between performance phase (learning vs. rehearsal) and drug (control vs. cuprizone) to predict success rate ($F(1) = 4.62$, $p = 0.04$). While control and cuprizone mice do not differ in success rate during pre-cuprizone learning, control mice perform significantly better during rehearsal relative to cuprizone-treated mice (Tukey's HSD, $p = 0.0004$). Both cuprizone and cuprizone-treated mice have improved performance during rehearsal relative to learning ($p = 0.0001$ and $p < 0.0001$, respectively). **h**, No relationship between peak oligodendrocyte loss post-cuprizone and peak reaching success rate during rehearsal. **i**, No relationship between rehearsal success rate and asymptote of oligodendrocyte replacement. *$p < 0.05$, **$p < 0.01$, ***$p < 0.001$. *Bars and errors represent Mean ± SEM, points represent individual mice, for statistics see* Supplementary Table 2.5.

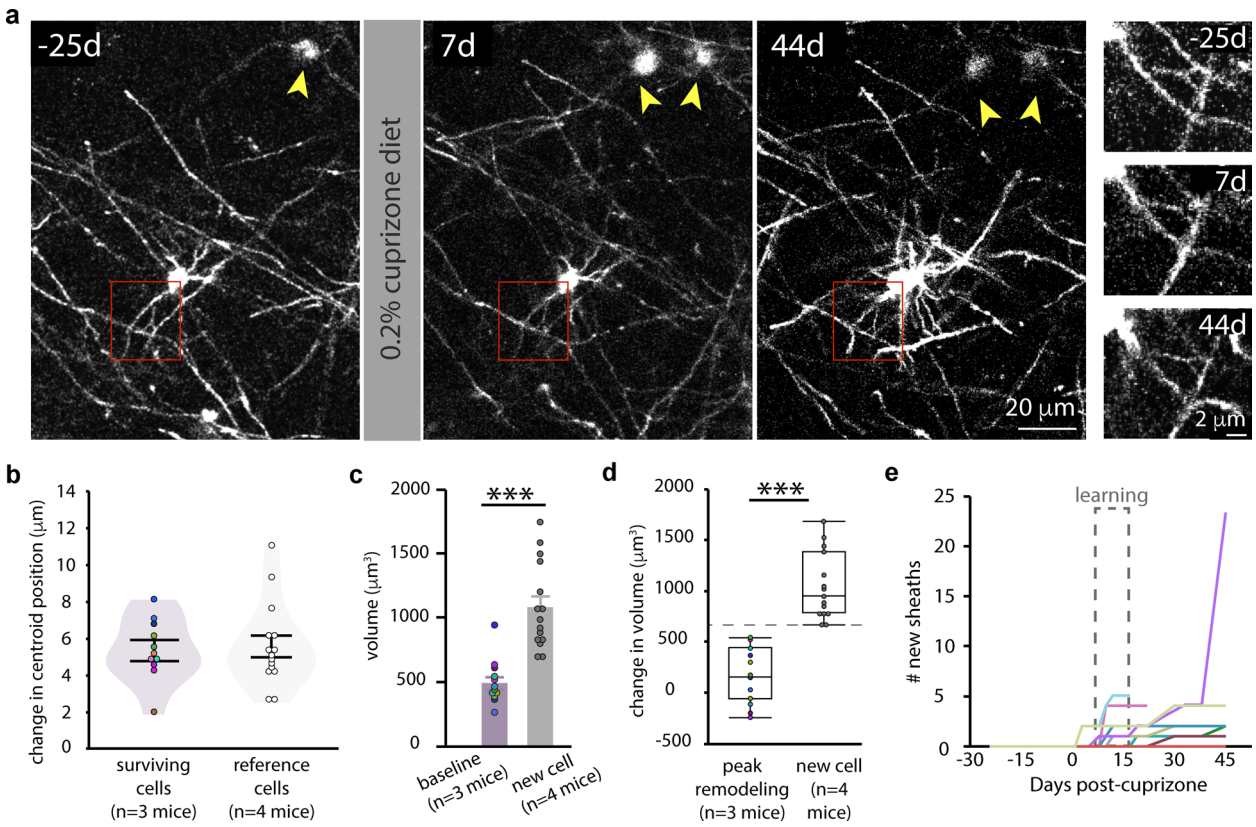

Extended Data Fig. 8 | Identification of oligodendrocytes that survive demyelination. a, Representative image outlining the methodology for following surviving oligodendrocytes over time. Single plane image of the same oligodendrocyte at baseline (−25d), one week after demyelination (7d), and six weeks after demyelination (44d). Red boxes highlight one example of the same oligodendrocyte processes lasting for the duration of the study. The maintenance of the spatial relationship between the oligodendrocyte of interest and other oligodendrocytes in the field of view (yellow arrowheads) provide further confirmation of oligodendrocyte identity. Note the new cell that appears at 7d. **b**, Change in centroid position of reference oligodendrocytes within the z-stack and surviving cell bodies from baseline to day of peak remodeling—that is the day where the largest number of sheaths were added by a given oligodendrocyte. **c**, Surviving oligodendrocytes at baseline are significantly smaller than new oligodendrocytes ($t(21.91) = -5.81$, $p < 0.0001$, Student's t-test). **d**, Change in volume of surviving oligodendrocytes from baseline to peak remodeling is significantly smaller than the volume of new oligodendrocytes ($t(23.88 = -7.59$, $p < 0.0001$). **e**, Dynamics of sheath addition over time. Each line represents an individual oligodendrocyte. *$p < 0.05$, **$p < 0.01$, ***$p < 0.001$. *Bars and errors represent Mean ± SEM, box plots represent Median and IQR, for statistics see* Supplementary Table 2.7.

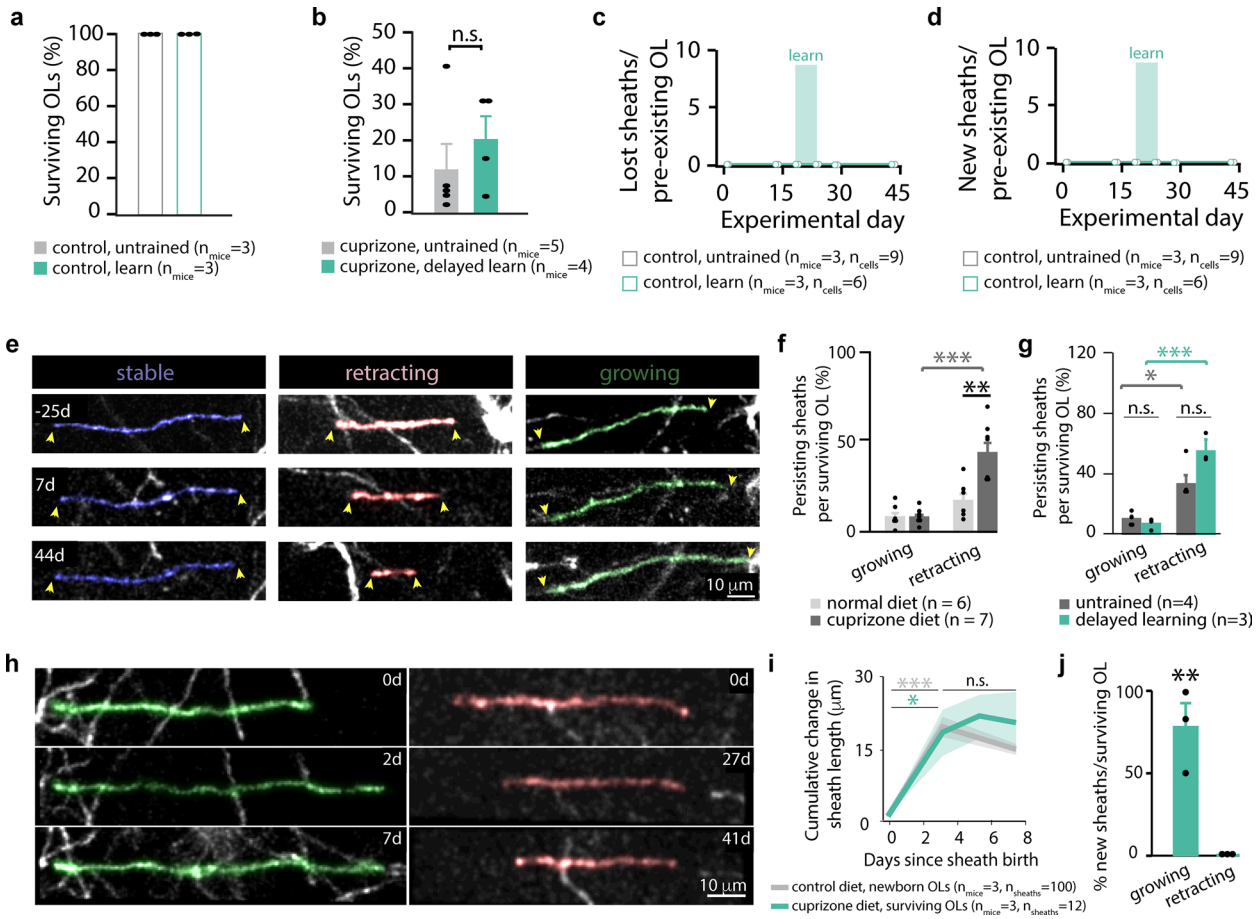

Extended Data Fig. 9 | Dynamics of pre-existing and newly-generated myelin sheaths from surviving oligodendrocytes. a, No oligodendrocytes are lost in healthy mice. **b**, No difference in percent of oligodendrocytes (OLs) surviving demyelination in untrained and delayed learning groups (Wilcoxon Rank-Sum, $p > 0.5$). **c, d**, No sheaths are lost (c) nor generated (d) on mature oligodendrocytes in healthy trained or untrained conditions. **e**, Behavior of pre-existing myelin sheaths that persist throughout study. Relevant sheaths are pseudo colored. **f**, Three weeks into remyelination, sheath retraction is significantly increased ($F(3,22) = 18.65$, $p < 0.0001$) when compared to age-matched controls (Tukey's HSD, $p = 0.0006$) and when compared to the percent of sheaths growing in cuprizone-treated mice ($p < 0.0001$). **g**, No effect of delayed learning on sheath dynamics during remyelination. Sheaths retract more than they grow in both untrained ($p = 0.016$) and delayed learning mice ($p = 0.0003$). **h**, Maximum projection of new sheaths generated after cuprizone exhibiting growth (pseudo colored green, left) and retraction (pseudo colored red, right). **i**, New myelin sheaths change in length in the week following their generation, whether they are from new oligodendrocytes (control: $F(3,302) = 47.94$, $p < 0.0001$) or from surviving oligodendrocytes after cuprizone-demyelination (cuprizone diet: $F(3,29) = 5.31$, $p = 0.0049$). Sheaths in both control and cuprizone treatment stabilize their length within 3 days of sheath birth (d0 vs. d3, $p < 0.0001$ in control and $p = 0.028$ in cuprizone; Tukey's HSD). Line and shading represent mean and SEM. **j**, Sheaths from pre-existing oligodendrocytes grow more often than they retract the first three days post-generation (Wilcoxon Rank-Sum, $p = 0.0029$). *$p < 0.05$, **$p < 0.01$, ***$p < 0.001$. *Bars and errors represent Mean ± SEM, for statistics see* Supplementary Table 2.7.

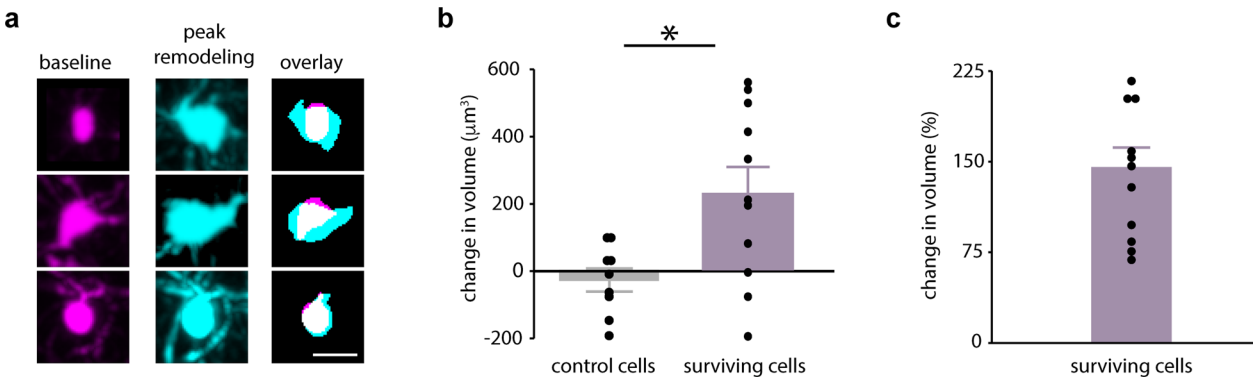

Extended Data Fig. 10 | Surviving oligodendrocyte cell soma volume changes during remyelination. a, Maximum projection of surviving oligodendrocyte cell bodies at baseline (left, magenta), peak remodeling (middle, cyan), and overlaid (right). Scale bar is 10 μm. **b**, Oligodendrocytes in normal untrained mice display little change in cell body volume throughout the study, from baseline (0d) to 43d. Surviving cells in delayed learning mice show dramatic increase in cell soma volume from baseline to day of peak remodeling when compared to oligodendrocytes in normal untrained mice ($t(12.24) = 2.56$, $p = 0.025$, Student's t-test). **c**, Percent change in volume between baseline and day of sheath addition for surviving cells engaging in remodeling. *$p < 0.05$, **$p < 0.01$, ***$p < 0.001$. *Bars and errors represent Mean ± SEM, for statistics see* Supplementary Table 2.7.

nature research

Corresponding author(s): Ethan Hughes

Last updated by author(s): 2020/03/24

Reporting Summary

Nature Research wishes to improve the reproducibility of the work that we publish. This form provides structure for consistency and transparency in reporting. For further information on Nature Research policies, see Authors & Referees and the Editorial Policy Checklist.

Statistics

For all statistical analyses, confirm that the following items are present in the figure legend, table legend, main text, or Methods section.

n/a	Confirmed	
☐	☒	The exact sample size (*n*) for each experimental group/condition, given as a discrete number and unit of measurement
☐	☒	A statement on whether measurements were taken from distinct samples or whether the same sample was measured repeatedly
☐	☒	The statistical test(s) used AND whether they are one- or two-sided *Only common tests should be described solely by name; describe more complex techniques in the Methods section.*
☐	☒	A description of all covariates tested
☐	☒	A description of any assumptions or corrections, such as tests of normality and adjustment for multiple comparisons
☐	☒	A full description of the statistical parameters including central tendency (e.g. means) or other basic estimates (e.g. regression coefficient) AND variation (e.g. standard deviation) or associated estimates of uncertainty (e.g. confidence intervals)
☐	☒	For null hypothesis testing, the test statistic (e.g. *F*, *t*, *r*) with confidence intervals, effect sizes, degrees of freedom and *P* value noted *Give P values as exact values whenever suitable.*
☒	☐	For Bayesian analysis, information on the choice of priors and Markov chain Monte Carlo settings
☐	☒	For hierarchical and complex designs, identification of the appropriate level for tests and full reporting of outcomes
☐	☒	Estimates of effect sizes (e.g. Cohen's *d*, Pearson's *r*), indicating how they were calculated

Our web collection on statistics for biologists contains articles on many of the points above.

Software and code

Policy information about availability of computer code

Data collection	Zen 2012 SP5 (Black, Zeiss), Cheetah (version 6.2.0, Neuralynx), Prairie View (version 5.4, Bruker)
Data analysis	Matlab (version 17a, Mathworks; custom code), Prism (version 8, Graphpad), JMP Pro (version 14, SAS), FIJI/ImageJ (1.45r-1.50i; custom code), Spike Sort 3D (version 2.5.4, Neuralynx)

For manuscripts utilizing custom algorithms or software that are central to the research but not yet described in published literature, software must be made available to editors/reviewers. We strongly encourage code deposition in a community repository (e.g. GitHub). See the Nature Research guidelines for submitting code & software for further information.

Data

Policy information about availability of data

All manuscripts must include a data availability statement. This statement should provide the following information, where applicable:

- Accession codes, unique identifiers, or web links for publicly available datasets
- A list of figures that have associated raw data
- A description of any restrictions on data availability

A summary of all data generated in this study is available in Supplementary Table 2. All raw data are publicly available upon request to corresponding author.

Field-specific reporting

Please select the one below that is the best fit for your research. If you are not sure, read the appropriate sections before making your selection.

☒ Life sciences ☐ Behavioural & social sciences ☐ Ecological, evolutionary & environmental sciences

Life sciences study design

All studies must disclose on these points even when the disclosure is negative.

Sample size	No statistical methods were used to predetermine sample sizes, but sample sizes used in this study are comparable to those reported in previous publications (see References 9,23)
Data exclusions	Three pre-established exclusion criteria were used in this study. 1) Mice were not included in remyelination analyses of post-cuprizone learning (Fig 6) if their mean success rate during learning was under 10%, to ensure that our behavioral intervention during remyelination was specific to mice able to perform the task. 2) Mice were excluded from 2-photon imaging components of the experiment if their cranial windows did not allow for clear visibility down to 336 microns of cortical depth at the onset of the experiment, or if they lost this clarity within the first four weeks of this experiment. This exclusion ensured that we could establish a consistent number of baseline cells from which to compare subsequent cell gain or loss. 3) To ensure that surviving oligodendrocytes were in fact individual surviving oligodendrocytes and not new oligodendrocytes generated in a similar location that myelinated similar axonal locations, we employed six criteria for inclusion in our final dataset: 1) Change in cell soma centroid (< 2.5 standard deviations from the mean) 2) Percentage of sheath retention (> 10% of original sheaths) 3) Change cell soma volume (< 700 µm3) 4) Protracted sheath addition (> 6 days) 5) Semi-automated tracing of new sheath to OL surviving cell body (using Simple Neurite Tracer) 6) Distance between surviving and new oligodendrocyte cell bodies at time point of sheath generation (> 50 µm)
Replication	We replicated experiments across multiple batches, where data were collected by multiple different experimenters. This allowed for successful replication across batch and experimenter. We then statistically controlled for inherent variation induced by batch effects using mixed modeling.
Randomization	Allocation of mice to experimental groups was random. However, due to the unpredictable nature of cranial window clarity and forelimb reach training success, we were unable to guarantee that each mouse allocated to a group would successfully complete the experiment. As a consequence, we were unable to guarantee that each replicate in the experiment contained all experimental groups. To account for this, we used statistical mixed modeling to control for variation induced by batch effects, and used appropriate normalization where possible.
Blinding	When possible, blinding to experimental condition was used in analyzing image stacks from two-photon imaging. We also conducted inter-rater reliability on a subset of images to ensure an absence of rater bias in cell counts, as described in the Methods section of this manuscript.

Reporting for specific materials, systems and methods

We require information from authors about some types of materials, experimental systems and methods used in many studies. Here, indicate whether each material, system or method listed is relevant to your study. If you are not sure if a list item applies to your research, read the appropriate section before selecting a response.

Materials & experimental systems

n/a	Involved in the study
☐	☒ Antibodies
☒	☐ Eukaryotic cell lines
☒	☐ Palaeontology
☐	☒ Animals and other organisms
☒	☐ Human research participants
☒	☐ Clinical data

Methods

n/a	Involved in the study
☒	☐ ChIP-seq
☒	☐ Flow cytometry
☒	☐ MRI-based neuroimaging

Antibodies

Antibodies used	All relevant information concerning antibodies used in this project can be found in Supplementary Table 1.
Validation	All validation information can be found in Supplementary Table 1, which contains relevant citations or links to relevant citations via antibody RRIDs.

Animals and other organisms

Policy information about studies involving animals; ARRIVE guidelines recommended for reporting animal research

Laboratory animals	All animals used in this study were aged 9-10 weeks at the start of the experimental time-lines described in Figs. 1-7. Males and females were used indiscriminately. C57BL/6N Charles River wild-type mice were used for electrophysiological experiments. NG2-mEGFP (Jackson stock #022735) and congenic C57BL/6N MOBP-EGFP (MGI:4847238) lines were used for two-photon imaging.

Wild animals	This study did not involve wild animals.
Field-collected samples	This study did not involve samples collected from the field.
Ethics oversight	All animal experiments were conducted in accordance with protocols approved by the Animal Care and Use Committee at the University of Colorado Anschutz Medical Campus

Note that full information on the approval of the study protocol must also be provided in the manuscript.